NASA Technical Memorandum 81494

MEASURED AND PREDICTED IMPINGEMENT NOISE FOR A MODEL-SCALE UNDER-THE-WING EXTERNALLY BLOWN FLAP CONFIGURATION WITH A QCSEE-TYPE NOZZLE

D.J. McKinzie, Jr.
Lewis Research Center
Cleveland, Ohio

June 1980

NASA

MEASURED AND PREDICTED IMPINGEMENT NOISE FOR A MODEL-SCALE UNDER-THE-WING EXTERNALLY BLOWN FLAP CONFIGURATION WITH A QCSEE-TYPE NOZZLE

by D. J. McKinzie, Jr.
National Aeronautics and Space Administration
Lewis Research Center
Cleveland, Ohio 44135

E-432

SUMMARY

The jet/flap interaction noise produced by a small-scale model of a two-flap, under-the-wing (UTW), externally blown flap (EBF) equipped with and without noise suppression devices was measured and predicted at jet Mach numbers of 0.5, 0.6, and 0.7. The devices consisted of short spanwise fairings centered in relationship to the jet axis and positioned in the slots between the wing and flaps. A nozzle approximating that of the Quiet Clean Short-Haul Experimental Engine (QCSEE) was located at nozzle to flap separation distances of nominally 5 and 4 nozzle diameters for the takeoff and approach attitudes, respectively. The study evaluated the noise suppression effectiveness of the spanwise fairings. In addition, static aerodynamic performance data were obtained.

In the takeoff attitude, the spanwise fairings produced OASPL noise reductions of 6 and 5 dB over a wide range of radiation angles in the flyover and sideline planes, respectively. These noise reductions were brought about by a modification in the boundary layer and shear layer velocity profiles at the trailing-edge of the most downstream flap due to the presence of the spanwise fairings. In the approach attitude, noise reductions of 5 dB occurred in the forward quadrant of the flyover plane only; in the sideline plane effectively no reductions were obtained.

The noise produced by the unsuppressed and suppressed configurations was modeled by assuming that the dominant noise sources were uncorrelated, thus permitting the sound field to be approximated by the superposition of separate noise source models. The calculated total noise compared favorably with the measured data in magnitude and trend. An analysis of the noise source mechanisms showed that the dominant noise appears to emanate from three principal sources. The first, trailing-edge noise, is produced by the jet flow passing over the trailing-edge of the most downstream flap. The second, fluctuating lift noise, is produced by the jet exhaust in-flow about the wing and flaps, which in turn produces a fluctuating lift response to an upwash disturbance. The third, impact noise, is produced by the jet exhaust impinging on the surface of the second flap. Two forms of the fluctuating lift component were derived and are referred to herein as the weak or strong interaction form of fluctuating lift. Conceptually, the strong interaction form is based on the assumption that a finite num-

ber of large-scale turbulence structures, varying over a small range of wave numbers, interact with the wing and flaps and thus produce noise. The weak interaction form is based on the assumption that a single large-scale turbulence structure interacts with the wing and flaps.

In the takeoff attitude comparison between the aerodynamic performance parameters obtained with and without the short spanwise fairings showed no significant differences. However, in the approach attitude, the fairings produced a 6-percent reduction in the flow turning efficiency.

INTRODUCTION

Experimental jet/flap interaction noise programs (refs. 1 to 3) have been conducted using scaled model nozzles with various engine under-the-wing (UTW) externally blown flap (EBF) configurations. In reference 2, a parametric study was made including some variations in the nozzle diameter and its location in relationship to the wing and flaps. However, the wing and flap scaled model configurations used in references 1 to 3 did not approximate the under-the-wing version of the Quiet, Clean, Short-Haul, Experimental Engine (QCSEE) powered-lift concept (ref. 4). This concept employs a low-pressure ratio fan resulting in a high bypass ratio turbofan engine. The QCSEE engine has a very large exhaust nozzle diameter of nominally 1.83 meters, some 2.77 times as large as the 0.66-meter diameter nozzle upon which the scaled model tests in references 1 to 3 were based. A typical QCSEE-type configuration is shown in figure 1 positioned in the takeoff attitude.

The QCSEE program was initiated to develop a suitable propulsion technology base for future powered-lift, short-haul aircraft (ref. 4). A factor that emerged from the studies was the need for low-pressure ratio fans in order to meet the noise goal. These pressure ratios were significantly lower than those used in most aircraft engines. Low fan pressure ratios result in high bypass ratio turbofan engines, which characteristically have low fan and core engine exhaust velocities and large exhaust nozzle areas. These lower exhaust velocities reduce the jet/flap interaction noise that is a major noise source for powered-lift aircraft, but the larger engine exhaust areas and their consequent flow fields tend to partially offset this benefit.

Since the completion of the tests reported in references 1 to 3, several empirical and/or semi-empirical acoustic analyses have been presented which predict the jet/flap interaction noise (refs. 5 to 8). A consideration of the analyses presented in references 5 and 6 indicate that if the separation distance between the plane of the nozzle exit and flap remains constant while the nozzle exit diameter is increased significantly several flow parameters will be altered. These parameters include the turbulence intensity, the width of the flow field as the flow passes over the wing and flap system, and the large-scale turbulence

structures (ring vortices), which are characterized as being the size of the entire flow field. In addition, because of the much larger engine exhaust flow field, not only are the flaps involved as noise sources, but the wing becomes an additional noise source. Until now, no experimental acoustic measurements have been published for such a configuration. In reference 9, the acoustic design features and techniques employed in the QCSEE propulsion system program were described. In order to meet the rather stringent sideline noise goal of 95 EPNdB at 152 meters, the jet/flap interaction noise design levels for takeoff and approach were shown to require noise suppression of at least 3.5 dB.

The first of four objectives of this study, conducted at the NASA Lewis Research Center, was to measure the noise produced by a two-flap scale model of the EBF configuration which approximates the QCSEE configuration in both the takeoff and approach attitudes. A second objective was to apply a noise prediction method presented in reference 6 to the measured test results in the flyover plane for both the takeoff and approach attitudes. In reference 6, the prediction method was specifically applied to an UTW EBF configuration oriented in the approach attitude, therefore, modifications of the derivation are presented herein in order to apply the method to the takeoff attitude. The third objective of the study was to determine the extent that the EBF noise could be suppressed using a suppression device presented in reference 6, and to apply the appropriate noise prediction expressions in order to aid in understanding the noise reductions produced by the treated configuration. Finally, the fourth objective was to present static aerodynamic performance data including the jet exhaust turning angle and turning efficiency for the configurations tested.

A comparison of the model reported on herein and the full-scale QCSEE-UTW EBF configuration oriented in the takeoff and approach attitudes is presented in figures 2 and 3, respectively. The nozzle-to-flap separation distances for the simulated takeoff and approach attitudes were set at nominally 5 and 4 nozzle diameters, respectively. The greatest difference between the model and full-scale configurations occurs in the takeoff attitude. This difference exists mainly in a larger separation distance between the nozzle exit plane and the second flap (most downstream flap) of the EBF configuration. This difference, of nominally one half nozzle diameter, is not considered of major importance in the production of noise. The model scale data were obtained at jet exhaust Mach numbers of 0.5, 0.6, and 0.7.

APPARATUS

The following section describes the test facilities and instrumentation used to obtain the acoustic and aerodynamic performance data presented herein, and the configurations tested.

Test Facilities

Anechoic chamber flow system. - The test stand, used to obtain the noise data presented in this report, was located in the Lewis Research Center Engine Fan and Jet Noise facility, shown schematically in figure 4. The mass flow metering system supplying cold air to the stand included a 10-centimeter flow control valve and flow metering run containing a 4.34-centimeter diameter orifice plate. The valve noise quieting elements in the flow system were a perforated plate followed by a 24.5-centimeter diameter, tubular, no-line-of sight muffler. As discussed in reference 10, jet noise test data obtained with this rig are not affected by internal valve noise to velocities as low as 120 m/sec. The acoustic measurements were made at jet Mach numbers of 0.5, 0,6, and 0.7. The flow data were taken at total temperatures which varied throughout the test between 290 K and 298 K; the anechoic chamber ambient temperature varied between 282 K and 298 K.

Acoustic instrumentation. - Twelve condenser-type microphones (0.64 cm diameter) were placed along the periphery of a 4.57-meter-radius horizontal semicircle, centered on the nozzle exit plane (fig. 4). The microphones were in a plane level with the nozzle centerline which is nominally 3.05 meters above the top of the fiberglass-type acoustic wedges on the floor of the facility. The data were taken in the plane of the nozzle axis perpendicular to the wing representing the flyover plane, and at an angle ϕ' of 22° below a plane passing through the jet axis and parallel to the wingspan representing the sideline plane. The 22° angle of the sideline plane, ϕ', represents the angle subtended by an aircraft located at an altitude of approximately 61 meters and at a sideline distance of 152.4 meters. For the takeoff attitude, the microphones were located at radiation angles, θ of 40°, 60°, 70°, 80°, 90°, 100°, 110° 120°, 130°, 140°, 150°, and 160° measured from the upstream nozzle axis for both the flyover and sideline tests. For the approach attitude, the microphones were located at θ of 40°, 50°, 60°, 70°, 80°, 90°, 100°, 115°, and 120° for both the flyover and sideline tests. With exceptions in the flyover plane at θ of 160° and 120° for the takeoff and the approach attitudes, respectively, the microphones were operated without grids. Grids and wind screens were necessary for the 120° and 160° microphones because the outer edge of the jet shear layer, deflected by the EBF model, intercepted these microphones.

The condenser microphones were calibrated before each day of testing, and the one-third octave band analyzer was calibrated each day with a white noise source between 200 hertz and 100 kilohertz.

Lift and thrust facility. - Static thrust and lift measurements were taken in the facility described in reference 11. The test stand was supplied by pressurized air at about 283 K. The air was supplied to a 15.25-centimeter diameter cylindrical plenum by two opposed supply lines. Flexible couplings, in each supply line, isolate the supply from a force measuring system. The plenum and any hardware attached to it is free to move

axially and laterally because of an overhead cable suspension system. The nozzle and wing/flap models were attached to the plenum at the downstream end with the span of the wing in the vertical plane. The axial thrust was measured by a load cell at the upstream end of the plenum. Horizontal sideloads (normal forces to the jet axis) were measured by a second load cell mounted closer to the nozzle.

Model Description

Nozzle. - A convergent circular nozzle having a nominal 10.1-centimeter diameter was used to simulate a jet engine nozzle in these tests (fig. 5). Four equally spaced pins 0.5 centimeter long by 0.5 centimeter in diameter were positioned in the exit plane of the nozzle which had a throat diameter of 10.1 centimeters and a nominal length of 20.6 centimeters. The nozzle including the pins was especially designed to inhibit the feedback mechanism of jets (ref. 12) which occurs at nozzle-to-flap separation distances less than or equal to 5 nozzle exit diameters. Based on calibrated mass flow measurements, the effective throat diameter of the nozzle was 9.3 centimeters.

EBF configurations. - The four variations of the UTW EBF configuration used in this study are shown schematically in figures 6 and 7. The model wing had a 32-centimeter chord with the flaps retracted and a 61-centimeter span. The unsuppressed configuration is shown in figures 6(a) and 7(a) in the takeoff and approach attitude, respectively. The installation of a passive type of suppression device in the slots between the wing and flaps is shown in figures 6(b) and 7(b). The device is a short spanwise nonporous fairing. This configuration is referred to herein as the suppressed configuration, and the fairings are referred to as plug fairings. Fairings similar to these were used in the large-scale acoustic tests reported in reference 6 and the small-scale tests reported in reference 13. The plug fairings were centrally located, in relationship to the intersection of the nozzle axis with the flaps as shown in figure 8, and were designed to prevent most of the impinging jet flow from passing through the spaces between the wing and flaps. Thus, they redirected the jet flow over and downstream on the impingement side of the flaps.

DATA

Acoustic test data are presented for both the flyover and sideline planes. The sideline plane is that plane rotated 22° about the exhaust nozzle axis below a plane passing through the nozzle axis parallel to the wing span. Overall sound pressure levels (OASPL) for each configuration are presented as a function of radiation angle, θ. During takeoff and approach the portion of the aircraft noise footprint of particular interest lies between values of the radiation angle θ of 70° and 110°. Consequently, in order to show some spectral detail, free field spectral

data are presented for radiation angles of 70^{o}, 90^{o}, and 110^{o}. At these radiation angles in the forward, mid, and aft quadrants different sound sources are known to dominate (ref. 6). Thus, these data will illustrate the asymmetric nature of the sound field. The acoustic data were obtained at jet Mach numbers of 0.5, 0.6, and 0.7.

The noise data were analyzed by an automated one-third octave band spectrum analyzer which produced sound pressure level spectra, SPL, referenced to 2×10^{-5} N/m^2. These data were corrected for effects of atmospheric attenuation (ref. 14). The lossless data were summed between 200 hertz and 40 kilohertz to determine the overall sound pressure level, OASPL. The resulting data are considered to represent reliable free field data (ref. 15). Additional spectral data obtained above 40 kilohertz were taken at frequencies of 50, 63, and 80 kilohertz and appear on the SPL plots presented herein.

AERODYNAMIC RESULTS

Measured aerodynamic performance characteristics are presented in table I for each configuration in the form of a dimensionless lift coefficient, F_N/T, a dimensionless thrust coefficient, F_a/T, a flow turning efficiency, η, and the flow turning angle. The ideal thrust, T, was calculated using the ideal mass flow rate for a nozzle having a diameter of 10.1 centimeters. The flow turning angles are referenced to the downstream nozzle centerline axis. The data representing the suppressed configuration in the takeoff attitude (X/D of 4.9) from table I(a) indicate that the average value of the dimensionless thrust coefficient obtained at jet Mach numbers of 0.5, 0.6, and 0.7 did not change in comparison to the unsuppressed configuration, however, the dimensionless lift coefficient was smaller by 0.02. These resulted in a decrease in the flow turning efficiency of 1 percent and a decrease in the flow turnangle angle of 1.7 degrees. For the approach attitude (X/D of 4.0), the data in table I(b) indicate that the average thrust coefficient for the suppressed and unsuppressed configurations were the same. However, the average lift coefficient for the suppressed configuration was smaller than that for the unsuppressed configuration by less than 0.04. These resulted in a decrease in the flow turning efficiency of 6 percent and a decrease in the flow turning angle of 2 degrees. In summary, the aerodynamic performance characteristics for the unsuppressed and suppressed configurations in the takeoff attitude were substantially the same, while in the approach attitude the suppressed configuration produced an 8-percent decrease in the dimensionless lift coefficient resulting in a 6-percent reduction in the flow turning efficiency.

In flight, a flow field attachment problem may develop in the approach attitude when the unsuppressed configuration is equipped with plug fairings. In this case, the flow diverted from passing through the slots between the wing and flaps by the nonporous plug fairings may cause the entire flow field passing over the upper surface of the flaps to either

become unstable or to entirely detach. In this regard, the forward flight wind tunnel test results reported in reference 16 are of interest. As part of the noise reduction and aerodynamic performance study reported, the slots between the wing and the three flaps of an UTW EBF configuration in the approach attitude were covered by nonporous fairings in several combinations. The approach attitude of the three flap EBF configuration of reference 16 is similar to the approach attitude of the two flap EBF configuration reported on herein. The particular aerodynamic performance results obtained with the fairings positioned over the slots between the flaps, but not over the slot between the wing and the first flap, were mentioned specifically. Reference 16 indicates that with the slot open between the wing and first flap and a large flap deflection, the flow remained attached over the upper surface. In addition, reference 16 indicates that this same result occurred in the test reported by another investigator. Thus, the aerodynamic test results of reference 16 suggest that the use of a nonporous fairing located in the slot between the two flaps of the unsuppressed configuration would not produce a detached upper or suction surface flow problem in flight. Unpublished data were obtained from another configuration designed in an effort to insure flow attachment over the flaps. In this configuration, screens were substituted in place of the nonporous fairings so that a small amount of flow would pass over the upper surface of the flaps thereby establishing a boundary layer which in turn would insure an attached flow field in flight. A comparison of the acoustic results obtained for an unsuppressed configuration in the approach attitude equipped with nonporous fairings in the slots between the wing and flaps and that for the same configuration equipped with screens in the slots indicates that the use of screens in place of the nonporous fairings had the gross effect of producing moderate additional amounts of mid- through very high-frequency noise in the forward quadrant of the flyover plane and throughout the sideline plane with only small differences in the noise produced in the aft quadrant of the flyover plane. On the basis of these test results, it appears that a combination of a screen and nonporous fairing could ensure flow field attachment in the approach attitude, while still producing noise suppression. In this application, a nonporous fairing would be located in the slot between the flaps of the EBF and a screen would be positioned in the slot between the wing and first flap. In the case of the suppressed configuration, discussed in this report, the wind tunnel tests of reference 16 indicate that a flow attachment problem would not occur in the takeoff attitude.

ANALYSIS OF JET/FLAP INTERACTION NOISE

One of the objectives of this report is to apply the noise prediction method presented in reference 6 to the measured acoustic data presented herein. The final form of the mathematical expressions appearing in reference 6 represent a specific application of the method to the UTW EBF configuration oriented in the approach attitude. In order to apply the prediction method to the UTW EBF configuration oriented in the takeoff

attitude, a brief review of the method is presented. The primary purpose for developing the prediction method presented in reference 6 was to aid in understanding the noise producing mechanisms and to determine the physical parameters upon which the mechanisms depend, with the objective of devising schemes for suppressing the noise. The models of the individual noise producing mechanisms include the overall-sound-pressure-level (OASPL) estimates of trailing-edge noise, the noise resulting from fluctuating lift (inflow noise) of the wing and flaps, and impact noise. References 5 and 6 present a more detailed discussion and/or derivation of these individual noise sources. It is assumed herein, as in reference 6, that trailing-edge noise, impact noise, and fluctuating lift noise are the dominant noise sources. By assuming that the noise sources are uncorrelated, as proposed in reference 5, their combined sound field can be approximated by superposition. Therefore, the total OASPL is expressed as the anti-logarithmic sum of impact, trailing-edge (TE), and fluctuating lift (FL) OASPL as follows:

$$OASPL_{impinge} = 10 \log 10\left[\exp\left(\frac{OASPL_{impact}}{10}\right) + 10 \exp\left(\frac{OASPL_{TE}}{10}\right) + 10 \exp\left(\frac{OASPL_{FL}}{10}\right)\right] \quad (1)$$

This summation is referred to in this report as impingement noise. The following sections present analytical expressions in SI units used to estimate trailing-edge, fluctuating lift, and impact noise.

Trailing-Edge Noise

Trailing-edge noise was analyzed in reference 17 and shown to have a velocity dependence of U^5. It is estimated in this report from the theoretical approach of reference 17 in the form presented in equation (11) of reference 5.

It is assumed that a directed flow lies on the surface of a semi-infinite plane which is thin and rigid (see fig. 9). The phenomena of interest occur near or at the edge of the half-plane. Eddies in the flow are well within a wavelength of the edge. The observer is assumed to be in the far field, and the flow region is turbulent and at high Reynolds number. In figure 9, δ represents the thickness of the boundary layer; W is taken as the spanwise distance between the centerline and a point where the local velocity is equal to one-half the maximum velocity U_m of the shear layer at the trailing-edge; r is the distance to the observer measured from the trailing-edge of the half-plane; and the angles Ψ and ϕ locate, in cylindrical coordinates, the field point referenced to the edge of the plate.

The expression for trailing-edge noise is derived from Lighthill's analysis, in which the turbulence is divided into regions of perfect correlation where the size of each region is very much less than the acoustic wavelength. From these considerations, the overall sound pressure level of trailing-edge noise $OASPL_{TE}$ is given by:

$$OASPL_{TE} = 10 \log \frac{W\delta U_m^5}{r^2} + 10 \log \cos^2 \frac{\Psi}{2} + 10 \log \frac{1.15\times10^6 p^2}{c} \qquad (2)$$

The angle Ψ was determined graphically as a function of the acoustic radiation angle θ. It may, however, be crudely approximated by setting

$$\Psi \simeq \Psi_N + \theta$$

where Ψ_N represents the acute angle between the surface of the second flap and the jet axis (see fig. 9). The constant in the last term of equation (2) includes the normalized turbulence intensity, which is assumed in this analysis to have a magnitude of 0.1.

The mathematical expression for this component includes terms for the boundary layer height, δ, and spanwise wetted edge length, 2W. Because these terms are not easily estimated from purely theoretical considerations, they were evaluated with the aid of experimental data. These data appear in figures 10 and 11 for the unsuppressed configuration oriented in the takeoff and approach attitudes, respectively. A comparison between the boundary layer and shear layer velocity profiles obtained in the takeoff and approach attitudes shows distinct dissimilarities. For example, the peak of each velocity profile in the takeoff attitude (fig. 10(a)) occurs at a height, z, in the shear layer well above the boundary layer height, δ. Conversely, in the approach attitude (fig. 11(a)) the peaks occur at heights very nearly equal to the boundary layer heights. These dissimilarities indicate major differences exist between the jet flow fields passing over the second flap for the two conditions. Figures 10(b) and 11(b) present extensions of these profiles over a larger vertical distance, z, above the flap surface. In the case of the takeoff attitude, figure 10(b), a significant portion of the velocity profile is seen to be nearly symmetric about the location of the peak velocity. Conversely, in the case of the approach attitude, figure 11(b), the velocity profiles are more asymmetric. These dissimilarities suggest the following: first, that the symmetric velocity profiles in the shear layers (fig. 10(b)) are characteristic of a free jet, indicating that a large portion of the free jet is preserved as the flow field passes over the second flap of the EBF; and second, that the asymmetric shear layer velocity profiles (fig. 11(b)) are characteristic of a wall jet. Thus, in the case of the takeoff attitude, the flaps effectively turn the jet flow field through some small angle approximately equal to the incidence angle, Ψ_N, of the flap's surfaces; and in the case of the approach attitude, the jet flow field impacts the flaps, reorganizes on their surfaces,

and leaves the trailing-edge of the most downstream flap in the form of a wall jet at or approximately at the incident angle, Ψ_N, of the flap's surface. These dissimilarities in the velocity profiles indicate that significant acoustical differences in the trailing-edge noise component will exist between the takeoff and approach attitudes. Figures 10(c) and 11(c) present the spanwise velocity profiles obtained at the trailing-edge of the second flap for the unsuppressed configuration in the takeoff and approach attitudes, respectively. The experimentally determined lengths of the semi-spanwise wetted edge W appearing in equation (2) were nominally 6.32 and 9.6 centimeters for the takeoff and approach attitudes, respectively. In the Mach number range shown they appear to be nearly independent of velocity.

In the case of the suppressed configuration oriented in the takeoff attitude the boundary layer height, δ, and the length of the spanwise wetted edge, 2W, were evaluated from the experimental data presented in figure 12. The shear layer velocity profiles obtained at the trailing-edge of the second flap covering a larger range of vertical height, z, than that covered in figure 12(a) are presented in figure 12(b). These profiles are symmetric about the peak velocity over a broad range of velocities. A comparison of these velocity profiles with the velocity profiles presented for the unsuppressed configuration (fig. 10(b)) in the takeoff attitude indicate that the suppressed configuration is turning the jet flow field more effectively, as a whole, than the unsuppressed configuration. This phenomena is due to the plug fairings positioned in the slots between the wing and flaps which redirect the flow that would otherwise pass through the slots between the flaps. For the takeoff attitude, the experimentally determined lengths of the semispanwise wetted edge W were nominally 7.26 centimeters. The values of δ and W used in the evaluation of the trailing-edge components of the noise in the approach attitude were found to be the same as those used for the unsuppressed configuration in the approach attitude presented in figures 11(a) and 11(c), respectively.

Fluctuating Lift Noise

A derivation of the noise produced from inflow effects is given in reference 6. The derivation is based on reference 18, in which an estimate of the dipole noise is presented for cases in which the source is considered intermediate between satisfying the conditions for compactness and noncompactness. One of the primary assumptions made in the derivation is that the large-scale turbulence structures of the nozzle flow field (ring vortices) are responsible for what is referred to as fluctuating lift noise (inflow noise). It is speculated in reference 5 that these structures could interact with the flaps of the UTW EBF in an aerodynamic sense and result in unsteady inflow about the flaps. This in turn could cause a fluctuating lift response, which would have an influence on the production of noise. This speculation is, in part, based on observations made of the large scale turbulence structures in jet flow fields (refs. 12 and 19).

In brief, the analysis of reference 18 considers a rigid airfoil immersed in a subsonic turbulent inflow. For the special case when the characteristic size of the turbulent structures is not small with respect to the chord length of the airfoil, it is suggested that an application may be made of some form of a quasi-steady solution describing the lift fluctuations. Once the lift fluctuations are described, the surface may be modeled as a small (i.e., small with respect to a wavelength) spherical source, and the point dipole expression may be modified to account for reduced radiation at acoustic wavelength to body size ratios which are small with respect to the chord. From these considerations, the overall sound pressure level of fluctuating lift noise $OASPL_{FL}$ for an EBF in the approach attitude is given as follows:

$$OASPL_{FL} = 10 \log \left[\frac{\left(C_{L_\alpha}\right) \rho_\ell U_\ell^2}{r} \right]^2 + 10 \log A_c \left(\frac{A}{A_c} \right) + 10 \log \left[\frac{A}{A_c} \left(\frac{\pi}{\frac{7.559}{M_\ell^2} + 1} \right) \right]$$

$$+ 10 \log \left[\frac{\frac{v'}{U_\ell}}{8\pi P_{ref}} \right]^2 + 10 \log \cos^2 \beta + 10 \log(0.23 f_r) \qquad (3)$$

Equation (3) was specifically derived assuming that the large-scale turbulence structures in the jet flow field are responsible for the generation of fluctuating lift noise. These turbulent structures are known to be among the so-called energy-bearing eddies of the jet flow field turbulence spectrum. They have been shown in reference 20 to be correlated with the low frequency noise produced by a jet impinging on a large wall. In applying equation (3) to the specific configurations described herein, some discussion of the inherent assumptions made in its derivation must be stated. These assumptions have not been explicitly presented previously, though they are implicit in the mathematical development of equation (3) presented in reference 6.

Discussion of assumptions. - Figure 13 is a schematic representation of the interaction between the large-scale turbulent structures and the EBF unsuppressed configuration in the approach attitude. For the purpose of this discussion, the turbulence structures are simply represented as toroidal vortex rings which are shown being convected downstream by the jet flow field, and thus expand and grow in size as the jet mixing layer grows. These large-scale turbulence structures extract energy from the mean jet flow, and this gain is balanced by viscous dissipation in the self-preserving flow field which starts at a point downstream from the nozzle exit greater than 5 nozzle diameters. Thus, between the nozzle

exit and at least 5 nozzle diameters downstream, the turbulent energy spectrum would be expected to be dominated by the energy contribution of the large-scale turbulence structures. As noted in figures 6(a) and 7(a), the flaps of the EBF configuration are coincidentally located within this same inhomogeneous region, for example, within 5 nozzle diameters of the nozzle exit plane. Therefore, it is assumed that these energy-bearing eddies are involved directly in the generation of the fluctuating lift component of the noise, and are represented as a small finite ensemble having lateral dimensions approximately the size of the flow field. Further, the wave number bandwidth of these eddies is assumed correlated directly with the acoustic output generated during the eddy/surface interaction. For the sake of simplicity, the bandwidth of the acoustic output is assumed to be a single one-third octave band centered on the frequency f_r. Where f_r, as derived in reference 6, is shown to be a direct function of the local jet velocity, U_ℓ, and an inverse function of the characteristic eddy length scale of the large-scale turbulence structures. These length scales are in turn shown to be a function of the local jet flow field diameter and thus the jet nozzle diameter. Therefore, for a constant velocity, U_ℓ, the magnitude of f_r changes inversely with nozzle diameter, D. As a result, in a small-scale application where D is small f_r becomes large and the last term of equation (3) contributes in a significant way to the OASPL. Conversely, for a large-scale application where D is large f_r becomes small and the last term of equation (3) contributes very little to the OASPL. As a consequence, in a large-scale application the OASPL approaches a dependence on the sixth power of the jet velocity and the second power of the nozzle diameter.

Application to the approach and takeoff attitudes. - In the case of the approach attitude (fig. 13), it is clear that as the ring vortices interact with the wing and flaps, the degree of interaction differs. In the case of the second (most downstream) flap, the entire flap appears to be periodically engulfed by the ring vortex as it moves downstream. This type of interaction is referred to here as a strong interaction. Conversely, in the case of the wing and first flap only the outer most portion of the ring vortex, and thus the flow field, is intermittently interacting in a grazing fashion. This type of interaction is referred to here as a weak interaction. This variation in the degree of interaction suggests that the level of the noise produced by the wing and flaps, and thus the mathematical expressions representing their noise levels, will vary. Because of the apparent strong interaction that takes place between the large-scale turbulence structures and the second flap, it is assumed that equation (3) approximates the fluctuating lift noise produced by the second flap. Since f_r is shown to be a direct function of the local jet velocity and an inverse function of the nozzle diameter, the expression for the fluctuating lift with strong interaction of the large-scale turbulence then coincidentally has an overall dependence on the seventh power of the velocity and the first power of the jet nozzle diameter. In the case of the wing and first flap, it is assumed that only

the largest (single) scale turbulence structure having a lateral diameter equal to the local flow field acts as an effective forcing function responsible for producing the fluctuating lift noise. Therefore, the last term on the right-hand side of equation (3) will be dropped resulting in a tonelike expression. This expression then represents the fluctuating lift noise produced by a weak interaction between a single large-scale turbulence structure and the wing and first flap. The resulting expression in the flyover plane is given by

$$OASPL_{FL} = 10 \log \left[\frac{\left(C_{L_\alpha}\right) \rho_\ell \Gamma_\ell^2}{r} \right]^2 + 10 \log A_c \left(\frac{A}{A_c} \right) + 10 \log \left[\frac{A}{A_c} \left(\frac{\pi}{\frac{7.559}{M_\ell^2} + 1} \right) \right]$$

$$+ 10 \log \left[\frac{\frac{v'}{U_\ell}}{8\pi P_{ref}} \right]^2 + 10 \log \cos^2 \beta \qquad (4)$$

In the takeoff attitude, the wing and both flaps of the unsuppressed configuration are grazed by the large-scale eddies, as shown schematically in figure 14. Thus, equation (4) represents the fluctuating lift noise resulting from the weak interaction of the large-scale turbulence structures with the elements of this wing/flap system with the result that the fluctuating lift noise displays an overall dependence on the sixth power of the velocity and the second power of the jet nozzle diameter.

Impact Noise

Although the specific mechanism which produces impact noise is not known, it is indicated in reference 5 that the large-scale turbulence structures present in the jet flow field may be involved. Therefore, the assumption is made in this analysis that impact noise is produced by the large-scale structures of the jet flow field impacting the flaps.

In the absence of an explicit theoretical expression, it is proposed, as in reference 5, that the small-scale test results of reference 21 along with additional unpublished data obtained with that facility be used to estimate the impact noise. In reference 21, the noise field produced when a jet impacted a very large smooth flat board is presented for several angles of incidence Ψ_N measured between the nozzle axis and the plane of the board. The noise field did not include leading- and trailing-edge

noise, but did include the remaining noise sources (i.e., oblique jet impingement coupled with surface viscosity effects, surface scrubbing, reflection by the surface, free jet mixing, and free shear layer mixing over the deflected flat surface). The test conditions of reference 21 included nondimensional geometric and fluid flow conditions similar to those of the tests described in this report. For convenience, the test results of reference 21 and the additional unpublished data applicable to the tests reported here are presented in tables II and III. Table II contains data applicable to the takeoff ($\Psi_N = 20^o$) attitude, and table III contains data applicable to the approach ($\Psi_N = 60^o$) attitude. The test results show that the directivity pattern is a function of angle of incidence, Ψ_N. It will be noted that these data are presented as a function of impingement velocity. The impingement velocity represents the velocity on the axis of a free jet at the streamwise station corresponding to the location of the impact surface. The data in tables II and III were obtained for nozzle to flap separation distances of 7 and 4 nozzle diameters, respectively. Since the separation distances for the takeoff and approach attitudes, considered here, are nominally 5 and 4 nozzle diameters, respectively, it would seem necessary to adjust the noise levels for the takeoff configuration ($\Psi_N = 20^o$, table II) for this difference. However, it is assumed here that since the data are presented as a function of impingement velocity, rather than jet exit velocity, that the corrections to the noise levels will be small. That is, it is assumed herein that for the same impingement velocity only small differences in impact noise are produced between nominal separation distances of 5 and 7 nozzle diameters.

In general, there is a difference between the magnitude of the incidence angle, Ψ_N, of the flat board data, presented in tables II and III (representing the impact noise), and the measured aerodynamic performance flow turning angles for each configuration presented in table I. This difference necessitates that a correction be made to the experimentally determined data used to represent the impact noise component in the analysis. This is necessary because the acoustic directivity is strongly related to the flow turning angle of a jet impacting a very large board as described in reference 21. The correction is generally applied by increasing the radiation angles, θ, appearing in tables II and III, by the difference between the incidence angle, Ψ_N, and the flow turning angle determined experimentally for the takeoff and approach attitudes. In the form of an equation, it is as follows:

$$\theta' = \left[\Psi_N - (\text{flow turning angle})_{\text{table I}}\right] + \theta_{\text{tables II and III}} \quad (5)$$

where θ' represents the corrected radiation angle.

NOISE SUPPRESSION RESULTS

This section presents a comparison between the OASPL produced by the unsuppressed and suppressed configurations in the takeoff and approach attitudes. Also included is a comparison between the spectral data produced by these configurations at a jet Mach number of 0.6. These latter data are included in order to supply typical detailed spectral information revealing the frequency ranges in which the noise reductions occur. A detailed discussion of the measured acoustic data obtained from the unsuppressed configuration is included in appendix A.

Overall-Sound-Pressure-Level Comparison Between Unsuppressed and Suppressed Configurations

Comparisons are presented at jet Mach numbers of 0.5, 0.6, and 0.7 between the OASPL data of the unsuppressed and suppressed configurations.

Takeoff OASPL directivity. - The comparison of the test results for the unsuppressed and suppressed configurations in the takeoff attitude are presented in figure 15. The data in the flyover plane (fig. 15(a)) show that nominal reductions in OASPL of 6 dB occurred between radiation angles θ, of 40° and 130° with smaller noise reductions between θ of 140° and 150°. It will also be noted that the peak noise produced by the suppressed configuration occurred at 150°. The data in the sideline plane (fig. 15(b)) show that nominal reductions in OASPL of 5 dB occurred between θ of 40° and 110° with progressively smaller reductions as θ increased from 120° to 150°.

Approach OASPL directivity. - The comparison of the test results for the unsuppressed and suppressed configurations in the approach attitude are presented in figure 16. The data in the flyover plane (fig. 16(a)) show that nominal reductions in OASPL of 5 dB occurred at jet Mach numbers, M_j, of 0.5, 0.6, and 0.7 between θ of 40° and 90°, 40° and 70°, and 40° and 60°, respectively. At θ above the upper limits of these ranges, the noise reductions progressively decreased, and at M_j of 0.6 and 0.7 the suppressed configurations generated small noise increases of nominally 1 dB. The data in the sideline plane (fig. 16(b)) show that only small reductions in OASPL of nominally 1 dB occurred between θ of 40° and 60° and between 90° and 110°. Elsewhere, small amounts of noise (nominally 1 dB) were generated above the unsuppressed configuration.

Spectral Comparisons Between Unsuppressed and Suppressed Configurations

Representative spectra of the suppressed configuration in the takeoff and approach attitudes are presented in figures 17 and 18, respec-

tively. Also shown for comparison are the spectra of the unsuppressed configuration. These representative spectra were obtained at M_j of 0.6 and present data obtained at θ of 70°, 90°, and 110° in the flyover and sideline planes.

Takeoff spectra. - In the flyover plane, figures 17(a) to (c), the largest noise reductions occurred in the mid-frequency range between 0.5 and 3.15 kilohertz. For example, at θ of 70° average noise reductions of 9 dB were obtained, while at 90° and 110° the reductions averaged 8 dB. In the low-frequency range, between 200 and 400 hertz, an average noise reduction of 4 dB was obtained. In the high-frequency range above 4 kilohertz, the noise reductions progressively decreased with both increased frequency and θ. For example, at θ of 70° and 90° the noise reduction decreased from a value of 7 dB at 4 kilohertz to zero at 80 kilohertz, while at 110° the noise reduction decreased from a value of 4.5 dB at 4 kilohertz to zero at 40 kilohertz with negligible amounts of noise generated above 50 kilohertz.

In the sideline plane, figures 17(d) to (f), the largest noise reductions again occurred in the mid-frequency range between 0.5 and 3.15 kilohertz, although the reductions were not as uniform throughout this frequency range as in the case of the flyover plane. For example, at θ of 70° and 90° the largest noise reductions occurred in the vicinity of the spectral peak and amounted to 8 dB, while at θ of 110° the largest reduction amounted to 6.5 dB. In the low-frequency range between 200 and 400 hertz, an average noise reduction of 4 dB was obtained. In the high-frequency range above 4 kilohertz, the noise reductions progressively decreased, as in the case of the flyover plane, with increased frequency.

Approach spectra. - In the flyover plane, figures 18(a) to (c), broadband noise reductions were obtained from the low- to high-frequency ranges at θ of 70° and 90° (figs. 18(a) and (b)). For example, noise reductions up to 6 dB were obtained in the vicinity of the spectral peaks in the mide-frequency range between 0.5 to 2.5 kilohertz. In the low-frequency range between 200 to 400 hertz average reductions of 2 and 3 dB were obtained at θ of 70° and 90°, respectively. In the high-frequency range above 2.5 kilohertz noise reductions decreased progressively with increased frequency from values of 6 and 2 dB at θ of 70° and 90°, respectively, to levels of noise generation of 2.5 and 2 dB, respectively, at 80 kilohertz. At θ of 110° (fig. 18(c)), however, only low-frequency noise reductions of nominally 2.5 dB were obtained between 200 and 500 hertz. Above 500 hertz, the suppressed configuration generated small amounts of noise, the largest amount being 3.5 dB at 4 kilohertz.

In the sideline plane, figures 18(d) to (f), only small amounts of noise reduction (nominally 1.5 dB) were obtained in the low- to mid-frequency range between 0.2 to 1.6 kilohertz. Above 2 kilohertz only negligible noise reductions were obtained at θ of 90° and 110° in contrast, at θ of 70° average noise increases of 2.5 dB were generated by the suppressed configuration.

COMPARISON OF PREDICTED AND MEASURED FLYOVER PLANE NOISE

In this section, the measured experimental acoustic data produced in the flyover plane by the unsuppressed and the suppressed configurations oriented in the takeoff and approach attitudes are compared with predicted values of the noise. These comparisons aid in understanding the noise source mechanisms associated with the unsuppressed configuration and demonstrate the extent to which the noise can be suppressed by the plug fairing noise suppression devices.

The measured data of the unsuppressed configuration are compared with an estimate of the total noise $OASPL_{impinge}$, (eq. (1)), where the total noise is calculated from the anti-logarithmic summation of trailing-edge noise, fluctuating lift noise, and impact noise.

The measured data of the suppressed configuration are compared with the anti-logarithmic summation of trailing-edge noise and impact noise. The fluctuation lift noise component is not included, because it is assumed that the nonporous plug fairings inserted between the flaps eliminate this noise component. The summation is expressed, therefore, by the following equation:

$$OASPL_{impact,TE} = 10 \log\left[10_{exp}\left(\frac{OASPL_{impact}}{10}\right) + 10_{exp}\left(\frac{OASPL_{TE}}{10}\right)\right] \qquad (6)$$

The calculated OASPL distributions expressed by either of equations (1) or (6) are compared with the measured data between radiation angles, θ, of 0^o and 160^o for the takeoff attitude and between θ of 0^o and 120^o for the approach attitude at jet Mach number, M_j, of 0.5, 0.6, and 0.7. Also included for each configuration are the experimentally determined values of the static aerodynamic performance parameters including the dimensionless thrust coefficient, F_a/T, dimensionless lift coefficient, F_N/T, the flow turning efficiency, η, and the flow turning angle.

Unsuppressed Configuration

The measured unsuppressed configuration OASPL directivities for the takeoff and approach attitudes are presented in figures 19 and 20, respectively. Also included are the theoretical estimates of trailing-edge noise (eq. (2)), fluctuating lift noise (eq. (3) or (4)) applied to the wing and both flaps, the corrected estimate of impact noise, and the impingement noise (eq. (1)). A discussion of the spacial evaluation of the parameters appearing in the expressions for these sound sources is presented in reference 6, and is amended in appendix B of this report.

Takeoff comparisons. - In figures 19(a), (b), and (c) the measured noise data and curves representing the takeoff attitude total noise prediction (impingement noise) and its components are shown at M_j of 0.5, 0.6, and 0.7, respectively. The calculated impingement noise (eq. (1)) is generally within ±1 dB of the measured data. At M_j between 0.5 and 0.7 the trailing-edge components of the noise are clearly dominant between θ of 0^o and nominally 100^o, the fluctuating lift components are generally dominant between θ of nominally 100^o and 125^o, and the impact components are dominant between θ of 125^o and 160^o. The trailing-edge components have a velocity dependence of U^5 as shown in equation (2), the weak interaction form of the fluctuating lift components have a velocity dependence of U^6 as shown in equation (4), and the impact components have a velocity dependence of U^8 as discussed in references 5 and 6. Thus, a major reduction in OASPL could be produced if the trailing-edge and impact components of the noise were reduced. The measured aerodynamic performance parameters presented in the tables on each of the figures 19(a) through (c) indicate that an average flow turning efficiency, η, of 77 percent was produced at an average flow turning angle of about 16 degrees.

Approach comparisons. - In figures 29(a), (b), and (c) the measured noise data and curves representing the calculated approach attitude total noise and its components are shown at M_j of 0.5, 0.6, and 0.7, respectively. The calculated impingement noise levels (eq. (1)) are, in general, 1.5 dB larger than the measured noise levels. At M_j between 0.5 and 0.7, the strong interaction form of the fluctuating lift components of the noise (eq. (3)) produced by the second flap are dominant between θ of 0^o and 80^o, and the impact components are dominant between θ of 100^o and 120^o. The strong interaction form of the fluctuating lift components of the noise estimated from equation (3) depend on a scaling law which predicts that the noise varies directly with the nozzle diameter, D, rather than D^2, which is the scaling law of the other noise sources considered here. Thus, as the model wing and nozzle are scaled up in size, the strong interaction form of the fluctuating lift component of the noise has a less dominant role in the total noise production than shown in figure 19 for the approach attitude. This does not, of course, occur in the case of the takeoff attitude where only the weak interaction form of the fluctuating lift applies. Between θ of 0^o and 60^o in figure 20, the trailing-edge components are secondary noise sources, yet these are more dominant than the weak interaction form of the fluctuating lift components produced by the wing and first flap, which have a velocity dependence of U^6 (eq. (4)). The measured aerodynamic performance parameters presented in figure 20 indicate an average flow turning efficiency, η, of 56 percent at an average flow turning angle of about 54 degrees.

In summary, the noise calculations made for the unsuppressed configuration indicate: first, that in the takeoff attitude the dominant component of the noise in the forward quadrant of the flyover plane is trailing-edge noise, while in the aft quadrant, the impact component is dominant; and second, in the approach attitude, the fluctuating lift component produced by the second flap is dominant in the forward quadrant, while the impact component is dominant in the aft quadrant.

Suppressed Configuration

In the takeoff attitude, the suppressed configuration has been shown in the Analysis of Jet/Flap Interaction Noise section to have more effectively turned the jet flow field as a whole than the unsuppressed configuration. Thus, in the limit of the small deflection angles characteristic of the suppressed configuration in the takeoff attitude, it was assumed that the impact component of the noise should approach jet noise as a lower limit with an additional allowance for reflection from the flaps hard surfaces. This assumption was justified by calculations made of the impact component using the data from table II which overestimated by from 2 to 3 dB the measured experimental data for the suppressed configuration. Therefore, in the takeoff attitude, the impact component of the noise was modeled using a free jet rotated through the average measured aerodynamic flow turning angle with the addition of 3 dB to account for the total reflection of the noise by the hard surfaces of the flaps. In the approach attitude, the curves representing the impact noise component include a correction to the radiation angles, θ, equal to the difference between the magnitude of the angle of incidence, Ψ_N, of the flat board data presented in table III and the measured aerodynamic performance flow turning angles, according to equation (5).

The measured OASPL directivities for the suppressed configuration in the takeoff and approach attitudes are presented in figures 21 and 22 respectively. Also presented are the calculated estimates of trailing-edge noise (eq. (2)), impact noise, and the anti-logarithmic sum of impact and trailing-edge noise ($OASPL_{impact,TE}$, eq. (6)). The fluctuating lift components of the noise are not included because the plug fairings are assumed to minimize or substantially eliminate inflow about the wing and flaps.

Takeoff comparisons. - In figures 21(a), (b), and (c) the measured noise data and curves representing the takeoff attitude $OASPL_{impact,TE}$ noise are shown at M_j of 0.5, 0.6, and 0.7, respectively. The calculated $OASPL_{impact,TE}$ noise (eq. (6)) is on the average 2 dB below the measured data. Though these levels are in fair agreement with the measured data and the general noise levels of both vary similarly with changes in M_j, an obvious, but small deviation in agreement as a func-

tion of θ is evident from the measured data. At each Mach number, the trailing-edge component is dominant between θ of 0^{o} and 80^{o}, and the rotated jet noise component is dominant in the region between θ of 100^{o} and 160^{o}.

OASPL noise reductions of nominally 6 and 5 dB in the flyover (fig. 15(a)) and sideline (fig. 15(b)) planes, respectively, were produced by the suppressed configuration. The principal cause of these significant noise reductions is related directly to the differences between the boundary layer heights, δ, and the local stream velocity, U_m, evaluated from the shear layer velocity profiles at the edge of the boundary layers for the unsuppressed and the suppressed configurations shown in figures 10(a) and 12(a), respectively. Specifically, a comparison between the trailing-edge noise components (eq. (2)) evaluated for each configuration at a jet Mach number of 0.6 (figs. 19(b) and 21(b)) indicates that the suppressed configuration (fig. 21(b)) produced a noise reduction of nominally 6.0 dB. Thus, the differences between the flow fields of the unsuppressed and suppressed configurations in the takeoff attitude produced suppression of the trailing-edge and impact components of the noise, which were both coincidently the dominant sources of the noise for the unsuppressed configuration.

Also presented in figures 21(a), (b), and (c) are the measured aerodynamic performance data for the unsuppressed and suppressed configurations. For the large reductions in noise mentioned above, only a small reduction of approximately 2 percent in flow turning efficiency, η, was produced by the suppressed configuration with a corresponding reduction of 1 degree in the flow turning angle.

Approach comparisons. - In figures 22(a), (b), and (c) the measured noise data and curves representing the approach attitude $OASPL_{impact,TE}$ noise at M_j of 0.5, 0.6, and 0.7, respectively, are presented. The calculated $OASPL_{impact,TE}$ noise (eq. (6)) is in good agreement with the measured data between θ of 40^{o} and 110^{o}. Between θ of 110^{o} and 120^{o}, however, the calculated noise levels underpredict the measured test data by up to nominally 2.5 dB at 120^{o}. The trailing-edge noise components are dominant between θ of 0^{o} and 40^{o}, and the impact components of the noise are dominant between θ of 60^{o} and 120^{o}.

Noise reductions of up to 5 and 1 dB occurred only in the forward qudrants of the flyover (fig. 16(a)) and sideline (fig. 16(b)) planes, respectively. The principal cause of these noise reductions is evident from a comparison of the calculated noise components in figures 20 and 22. First, the noise levels of the trailing-edge and impact components are effectively the same for the two configurations, thus, these noise components were unaffected by positioning the plug fairings in the slots between the wing and flaps of the approach attitude. Second, in the case of the unsuppressed configuration (fig. 20) the fluctuating lift compo-

nents of the noise produced by the second flap are the dominant sources of noise, however, in the case of the suppressed configuration (fig. 22) the fluctuating lift components of the noise produced by the wings and both flaps were eliminated by the plug fairings. Thus, the 5 dB noise reductions in the flyover plane were brought about by the plug fairings, which suppressed the fluctuating lift components of the noise. The most dominant component of the fluctuating lift was produced by the downstream flap.

Also presented in each figure are the measured aerodynamic performance data for the unsuppressed and suppressed configurations. A comparison between them indicates that the suppressed configuration produced a reduction of approximately 6 percent in turning efficiency, η, with a corresponding reduction in the flow turning angle of nominally 1.5 degrees.

CONCLUDING REMARKS

The present test results demonstrated that the plug fairings effectively suppressed the fluctuating lift components of the noise in the takeoff and approach attitudes with small reductions in the aerodynamic performance, for example, flow turning efficiencies and turning angles. In addition, in the takeoff attitude, the plug fairings produced an unexpected partial suppression of the trailing-edge and the impact noise components. This suppression is believed due to a modification in the boundary layer and shear layer velocity profiles at the trailing-edge of the second (most downstream) flap. The impact noise component was modeled by jet mixing noise rotated through the aerodynamic performance flow turning angle and increased by 3 dB for reflection by the hard surfaces of the flaps. This represents an example of the impact noise component approaching the asymptotic limit of jet noise when the angle of incidence between the jet axis and the impingement surface approaches a small value, as discussed in the Comparison of Predicted and Measured Flyover Plane Noise section.

One further remark should be made regarding the role that the large-scale enrgy bearing turbulence structures of the jet flow field have in the production of trailing-edge noise. As schematically depicted in figure 14, showing the unsuppressed configuration in the takeoff attitude, the large-scale turbulence structures are convected downstream and pass over the trailing-edge of the most downstream (second) flap. Since this same phenomenon occurs in the case of the suppressed configuration (fig. 6(b)), it is plausible to assume that the plug fairings located in the slots turn the jet more effectively than the flaps alone, with the result that the plug fairings help to maintain the integrity of the large-scale turbulence structures. This assumption is supported by comparing the shear layer velocity profiles for the unsuppressed and suppressed configurations presented in figures 10(b) and 12(b), respectively. These figures indicate that the shear layer velocity profiles of the suppressed configuration are more clearly similar to the free shear layer velocity

profiles of a pure jet flow field. If the plug fairings do, in fact, turn the jet more effectively, then it could be hypothesized that the large-scale turbulence structures in the jet flow field should interact as complete eddy structures with the trailing-edge of the most downstream flap and should contribute to the generation of trailing-edge noise. A comparison of the data in figures 19 and 21, showing the total measured noise produced in the takeoff attitude by the unsuppressed and suppressed configurations, respectively, clearly indicate that the suppressed configuration did not produce an increase in the measured total noise. Rather these data showed that the suppressed configuration produced a nominal 6.0 dB reduction in the measured total noise and also in the predicted trailing-edge component of the noise. These data, therefore, imply that the large-scale turbulence structures did not contribute to the generation of the trailing-edge noise. The cause of this apparent contradiction may be related to the lack of coherent whole body pressure and velocity fluctuation associated with the large-scale structures unsteady motion as it passes over the sharp trailing-edge of the most downstream flap.

SUMMARY OF RESULTS

The jet/flap interaction noise produced by a small-scale model of a two-flap, under-the-wing, externally blown flap equipped with and without a passive noise suppression device was measured and predicted. In addition, static aerodynamic performance data were measured. The following results were obtained:

1. Measured free-field OASPL and SPL acoustic data were obtained in both the flyover and sideline planes for an UTW EBF unsuppressed and suppressed configuration oriented in the takeoff and approach attitudes. Significant reductions of OASPL noise were produced by the suppressed configuration. In the takeoff attitude, the measured data show that noise reductions of 6 and 5 dB occurred over a wide range of radiation angles in the flyover and sideline planes, respectively. In the approach attitude, the measured data in the flyover plane show that noise reductions of 5 dB occurred over a broad range of radiation angles in the forward quadrant only. In the sideline plane effectively no reductions were produced in the forward or aft quadrants.

2. Two theoretically based noise source models and one empirically based model were combined to provide estimates of the flyover plane OASPL jet/flap noise produced by the unsuppressed and suppressed configurations in the takeoff and approach attitudes. The calculated relations compared favorably with the measured data in magnitude and trend. The individual noise source models included trailing-edge noise, fluctuating lift noise (inflow noise), and impact noise.

3. Two forms of the fluctuating lift component of the noise were presented. They are referred to as the weak and strong interaction

forms of fluctuating lift. They conceptionally represent: first, the interaction of a finite number of large-scale jet turbulence structures, varying over a small range of wave numbers, with the wing and flaps of the EBF (strong interaction); and second, the interaction of a single large-scale turbulence structures with the wing and flaps (weak interaction). In the expressions for the weak and strong interactions, the noise is shown to scale with either the sixth or seventh power of the jet velocity, respectively.

4. A comparison between the aerodynamic performance parameters obtained for the unsuppressed and suppressed configurations in the takeoff attitude showed that only small differences occurred in the flow turning efficiencies and turning angles. However, in the approach attitude, the suppressed configuration produced a 6-percent reduction in the flow turning efficiency.

APPENDIX A

UNSUPPRESSED CONFIGURATION DATA

The following presents the unsuppressed configuration data obtained in the form of OASPL directivities followed by a limited presentation of SPL spectra, representative of the forward ($\theta = 70^{\circ}$), mid ($\theta = 90^{\circ}$), and aft ($\theta = 110^{\circ}$) quadrants of the flyover and sideline planes.

Takeoff Attitude

OASPL directivity. - The OASPL distributions between radiation angles of 40° and 160° are presented for the flyover and sideline planes in figure 23 at nozzle exit Mach numbers, M_j, of 0.5, 0.6, and 0.7. In the flyover plane (fig. 23(a)), the data show similar changes in OASPL with radiation angle, θ, as a function of M_j for $40^{\circ} \leq \theta \leq 120^{\circ}$. However, between $120^{\circ} \leq \theta \leq 160^{\circ}$ there is a disproportionate increase in noise level with increased M_j. This increase indicates that a sound source is acting which has a greater dependence on jet velocity. The peak noise produced by the unsuppressed configuration in the takeoff attitude occurred at θ of 90°. In the sideline plane (ϕ of 68°, fig. 23(b)) the data show similar changes in OASPL with radiation angle, θ, as a function of M_j. The peak noise produced in the forward quadrant of the sideline plane occurred at θ of nominally 70°, while in the aft quadrant it occurred at θ of 160°.

Spectra. - The spectra representing the unsuppressed configuration in the takeoff attitude are presented in figure 24. These data demonstrate the broadband character of the sound field as a function of θ and M_j in the flyover and sideline planes.

In the high-frequency range between 4 and 40 kilohertz, the data have similar negative slopes of nominally 4 dB per octave.

In the low-frequency range between 200 and 400 hertz the greatest slopes of the data occur. For example, slopes of nominally 10 dB per octave occurred at θ of 70°, decreasing to 8 dB per octave at θ of 110°.

The frequencies at which the peak values of SPL occurred in the flyover plane (figs. 24(a) to (c)) changed as functions of θ and M_j. For example, at M_j of 0.5 and θ of 70° a conical shaped spectra peaked near 500 hertz. At θ of 90° and 110°, however, the spectral peaks have a broad or blunt shape appearing to have two peaks widely separated in frequency. At M_j of 0.7 and θ of 70° a tone appears to exist at a

frequency of 1250 hertz, while at θ of 90° and 110° the spectra show distinct peaks at 1600 hertz. Conversely, in the sideline plane (figs. 24(d) to (f)) the frequencies at which the peak values of SPL occurred are relatively insensitive to changes in radiation angle while showing a small increase in frequency with increased M_j.

Approach Attitude

OASPL directivity. - The OASPL distributions between θ of 40° and 120° are presented for the flyover and sideline planes in figure 25. In the flyover plane (fig. 25(a)) the data show similar changes in OASPL with θ as a function of M_j for $40° \leq \theta \leq 90°$. However, between $90° \leq \theta \leq 120°$ there is a disproportionate increase in noise level with increased M_j. The increase in noise level between θ of 90° and 120° indicates, as in the case of the takeoff attitude, that a sound source is acting which has a greater dependence on jet velocity. The peak noise produced by the unsuppressed configuration in the flyover plane of the approach attitude (fig. 25(a)) occurred at θ of nominally 60°. In the sideline plane (θ of 68°, fig. 25(b)) the data at M_j of 0.5, 0.6, and 0.7 show similar changes in OASPL between θ of 40° and 90°, with a slight spreading effect between θ of 100° and 120°. The peak noise produced in the sideline plane occurred in the forward quadrant at θ of 40°.

Spectra. - The spectra representing the unsuppressed configuration in the approach attitude are presented in figure 26. In the high-frequency range of the flyover plane between 6.3 and 50 kilohertz the data have negative slopes varying between 4 and 5 dB per octave at θ of 70° and 90°, and between 2 and 3 dB per octave at θ of 110°. In the sideline plane, the data at θ of 70°, 90°, and 110° have negative slopes varying between 2 and 4 dB per octave between frequencies of 4 and 50 kilohertz.

In the low-frequency range between 200 and 400 hertz, the largest slopes of the data occurred, similar to the takeoff attitude. For example, slopes of nominally 6 dB per octave typically occurred at M_j of 0.5, while at M_j of 0.7 they were nominally 10 dB per octave.

The peak frequencies and spectral shapes of the data in the flyover plane (figs. 26(a) to (c)) were distinctly different from those of the sideline plane (figs. 26(d) to (f)). For example, in the flyover plane, the spectral peak of the Mach number 0.5 data typically occurred at a higher frequency than that of the 0.7 Mach number data. Conversely, in the sideline plane, the spectral peaks of the data were very close to occurring at the same frequency independent of both M_j and θ. These differences in spectral peak frequencies were also accompanied by distinct differences in the broadband shapes of the spectra. For example, in the

flyover plane, the spectral shapes varied as a function of M_j and, in general, were irregular with several apparent peaks. However, in the sideline plane, the spectra displayed similar shapes as a function of M_j and were regular in shape with only a single peak occurring at a frequency of 1 kilohertz.

APPENDIX B

EVALUATION OF SOUND SOURCE PARAMETERS

Trailing-edge noise is calculated by using equation (2), where the boundary-layer height δ and spanwise wetted edge $2W$ are valuated at the trailing-edge of the second (most downstream) flap. The boundary-layer heights were determined by fitting the universal velocity distribution law presented in reference 23 and described in appendix C herein to the measured velocity profile data at the centerline point on the trailing-edge of the second flap in the z plane (fig. 9). The spanwise velocity profiles were measured at an arbitrary height above the impact surface beyond the boundary-layer height in the plane of the trailing-edge.

Fluctuating lift noise is calculated by using equation (3) for cases in which strong jet/flap interaction occurs, or equation (4) for the cases of weak interaction. The slope of the lift coefficient $\left(C_{L_\alpha}\right)$ in equations (3) and (4) is estimated by using equation (B14) from reference 6. With one exception, the various parameters appearing in equations (3) and (4) were evaluated as described in reference 6. The exception concerns the spatial location, in the case of the flaps, where the magnitude of the upwash turbulence intensity (v'/U_ℓ) was evaluated. Rather than at the same streamwise axial stations and radial locations off the jet axis corresponding to the mid-chord of the flaps, as suggested in referene 6, they were evaluated at the leading-edge of the flaps. In order to aid in evaluating the actual correlation area A and the turbulence intensity v'/U_ℓ, appearing in equations (3) and (4), curves are presented in figures 27 and 28, respectively. The correlation area A is defined as follows:

$$A = CL$$

where C represents the effective chord length of the airfoil, and L represents the lateral correlation length for oblique jet impingement of a large-scale turbulence structure against a flat surface (fig. 27). The curve in figure 27 is based on data presented in references 1, 23, and 24, and the method used to obtain it is described more fully in reference 6. In figure 28 the axial jet turbulence intensity, u''/U_j (fig. 28(a)), and the radial turbulence intensity, v''/U_j (fig. 28(b)), are presented. They were obtained from references 25 and 26, respectively, at a jet Mach number of 0.3. Before these values of the turbulence intensities can be used in equations (3) and (4), they must be transformed by factoring in the ratio U_j/U_ℓ presented in reference 27, which represents a correction for the decay of the mean jet exit flow velocity, U_j. Also, because the turbulence intensities are shown in reference 25 to be a function of the

jet Mach number, they must be corrected for differences in jet Mach number, if different from 0.3 , by the curves presented in figure 14 of reference 25. Impact noise is estimated from the experimental data of reference 21 along with additional unpublished data presented in tables II and III, which are applicable to the tests reported here, but must be corrected for scaling effects presented in reference 1.

APPENDIX C

UNIVERSAL VELOCITY DISTRIBUTION LAW

The magnitudes of the turbulent boundary layer thickness, δ, were determined by fitting the following expression for the logarithmic velocity distribution law to the measured velocity profile data.

$$\frac{U}{U_e}\sqrt{\frac{1}{C_f'}} = 4.137 \log \frac{y\, U_e\sqrt{C_f'}}{\nu(1.4142)} + 3.932 \qquad \text{(C-1)}$$

This expression represents the universal velocity distribution law presented in reference 21 for flow at very large Reynolds numbers along a flat plate. C_f' represents the local skin friction coefficient, and U_e is the local velocity of the flow at the edge of the boundary layer δ. Since the magnitude of local skin friction coefficients were unknown in the present tests, they were estimated by fitting equation (C-1) to the measured velocity distributions. Upon optimization of this procedure, the boundary-layer heights δ were estimated assuming that the velocity distributions, U/U_e, reached 0.99 at the edge of the boundary layers. Substitution of 0.99 for U/U_e into equation (C-1) results in

$$\sqrt{\frac{1}{C_f'}} = 4.179 \log \frac{\delta\, U_e\sqrt{C_f'}}{\nu(1.4142)} + 3.972 \qquad \text{(C-2)}$$

It should be mentioned that the magnitudes of the local skin friction coefficients C_f' determined in the above exercise were found to approximate those presented in table 21.1 of reference 22 for turbulent flow passing over a flat plate, where the values of C_f' presented in reference 22 are a function of Reynolds number based on surface length.

APPENDIX D

SYMBOLS

A	actual correlation area, m^2
A_c	ideal correlation area, $\pi \ell_1 \ell_2$, m^2
C	chord length, m
C_f'	local skin friction coefficient
$\left(C_{L_\alpha}\right)$	steady-state effective lift coefficient slope, deg^{-1}
c	speed of sound, m/sec
D	nozzle exit diameter, m
f	frequency, Hz
f_r	characteristic frequency of fluctuating lift forces, Hz
F_a	axial thrust, N
F_N	lift force normal to jet axis, N
L	lateral correlation length of large-scale turbulence structure on flap's impact surface (source dimension), m
ℓ_1	streamwise semiaxial length of ellipse (ref. 6), m
ℓ_2	spanwise semiaxial length of ellipse (ref. 6), m
M_j	jet exit Mach number
M_ℓ	local Mach number evaluated on jet axis
OASPL	overall sound pressure level, dB
P_{ref}	reference sound pressure, 20 $\mu N/m^2$
r	distance between observer and trailing-edge (fig. 9), or distance between observer and centerline of nozzle exit plane, m
SPL	sound pressure level, dB
T	ideal nozzle thrust, N
U	mean flow velocity, m/sec

U_e local mean flow velocity at edge of boundary layer, m/sec

U_ℓ local mean flow velocity evaluated on jet axis, m/sec

U_m mean velocity of free shear layer at edge of boundary layer m/sec

u'' axial component of turbulence velocity fluctuation, m/sec

v' resultant component of turbulence velocity fluctuation normal to airfoil chord and leading edge, m/sec

v'' radial component of turbulence velocity fluctuation, m/sec

W one-half of spanwise width of velocity profile between points where local maximum mean velocity is equal to U/2 at trailing-edge of flap, m

x,y,z Cartesian coordinates (fig. 9)

β angle between fluctuating force vector and observer, deg

δ thickness of boundary layer, m

θ radiation angle measured from nozzle inlet axis (fig. 4), deg

θ' corrected radiation angle (see eq. (5)), deg

ν kinematic viscosity, m^2/sec

η flow turning efficiency represents the square root of the sum of the square of the dimensionless lift, F_N/T, and dimensionless thrust, F_a/T

ρ density of undisturbed fluid, kg/m^3

ρ_ℓ density of fluid evaluated at point where U_ℓ is determined, Kgm/m^3

ϕ angle defined in fig. 9, deg

ϕ' angle defined in fig. 4, deg

Ψ angle defined in fig. 9, deg

Ψ_N angle of incidence between plane of the surface and the jet axis as defined in figs. 9 and 27, deg

Subscripts:

exp	exponential
FL	fluctuating lift
impact	impact
impinge	impingement
j	jet exit condition
ℓ	local
TE	trailing edge

REFERENCES

1. Dorsch, Robert G.; Kreim, Walter J.; and Olsen, William A.: Externally Blown Flap Noise. NASA TM X-67991, 1972.

2. Olsen, William A.; Dorsch, Robert G.; and Miles, Jeffrey H.. Noise Produced by a Small-Scale, Externally Blown Flap. NASA TN D-6636, 1972.

3. Dorsch, Robert G.. Goodykoontz, Jack H.; and Sargent, Noel B.: Effect of Configuration Variation on Externally Blown Flap Noise. NASA TM X-71495, 1974.

4. Ciepluch, Carl: QCSEE Program Background. Quiet, Powered-Lift Propulsion, NASA CP-2077, 1979, pp. 1-16.

5. McKinzie, Daniel J., Jr.; and Burns, Robert J.: Analysis of Noise Produced by Jet Impingement Near the Trailing-Edge of a Flat and a Curved Plate. NASA TM X-3171, 1975.

6. McKinzie, Daniel J., Jr.; Burns, Robert J.; and Wagner, Jack M.: Noise Reduction Tests of Large-Scale-Model Externally Blown Flap Using Trailing-Edge Blowing and Partial Flap Slot Covering. NASA TM X-3379, 1976.

7. Dorsch, Robert G.; Clark, Bruce J.; and Reshotko, Meyer: Interim Prediction Method for Externally Blown Flap Noise. NASA TM X-71768, 1975.

8. Fink, M. R.: A Method for Calculating Externally Blown Flap Noise. NASA CR-2954, 1978.

9. Loeffler, Irvin J.; Smith, Edward B.; and Sowers, Harry D.: Acoustic Design of the QCSEE Propulsion Systems. Powered Lift Aerodynamics and Acoustics, NASA SP-406, 1976, pp. 335-356.

10. Olsen, W.; Burns, R.; and Groesbeck, D. E.: Flap Noise and Aerodynamic Results for Model QCSEE Over-the-Wing Configurations. NASA TM X-73588, 1977.

11. von Glahn, U.; and Groesbeck, D. E.: Effect of External Jet-Flow Deflector Geometry on OTW Aero-Acoustic Characteristics. AIAA Paper 76-499, July 1976.

12. Neuwerth, G.: Acoustic Feedback Phenomena of the Subsonic and Hypersonic Free Jet Impinging on a Foreign Body. NASA TT F-15719, 1974. Transl. of Akustische Rueckkopplungserscheinungen am Unter- und Oberschall-Freistrahl, der auf einen Stoerkoerper trifft, Tech. Hochschule, Inst. fuer Luft und Raumfahrt, (Bachen), 1972.

13. McKinzie, Daniel J., Jr.: EBF Noise Suppression and Aerodynamic Penalties. NASA TM-73823, 1978.

14. Shields, F. D.; and Bass, H. E.: Atmospheric Absorption of High-Frequency Noise and Application to Fractional-Octave Bands. NASA CR-2760, 1977.

15. Wazyniak, Joseph A.; Shaw, Loretta M.; and Essary, Jefferson D.: Characteristics of an Anechoic Chamber for Fan Noise Testing. NASA TM X-73555, 1977.

16. Pennock, A. P.; Swift, G.; and Marbert, J. A.: Static and Wind Tunnel Model Tests for the Development of Externally Blown Flap Noise Reduction Techniques. (LG74ER0170, Lockheed-Georgia Co.; NASA Contract NAS3-16831.) NASA CR-134675, 1975.

17. Ffowcs Williams, J. E.; and Hall, L. H.: Aerodynamic Sound Generation by Turbulent Flow in the Vicinity of a Scattering Half Plane. J. Fluid Mech., vol. 40, pt. 4, Mar. 1970, pp. 657-670.

18. Hayden, Richard D.: Noise From Interaction of Flow With Rigid Surfaces: A Review of Current Status of Prediction Techniques. NASA CR-2126, 1972.

19. Kibens, V.: Discrete Noise Spectrum Generated by an Acoustically Excited Jet. AIAA Paper 79-0592, Mar. 1979.

20. Wagner, F. R.: The Sound and Flow Field of an Axially Symmetric Free Jet Upon Impact of a Wall. Z. Flugwiss., vol. 19, no. 1, Jan. 1971, pp. 30-44. Also NASA TT F-13942, 1971.

21. Olsen, William A.; Miles, Jeffrey H.; and Dorsch, Robert G.: Noise Generated by Impingement of a Jet Upon a Large Flat Board. NASA TN D-7075, 1972.

22. Schlichting, Hermann: Boundary Layer Theory. First Ed. Pergamon Press, 1955, p. 437.

23. Foss, John F.; and Kleis, Stanley J.: The Oblique Impingement of an Axisymmetric Jet. (AR-2, Michigan State University; NASA Grant NGR 23-004-068). NASA CR-134961, 1976.

24. Groesbeck, Donald E.; Huff, Ronald G.; and von Glahn, Uwe: Comparison of Jet Mach Number Decay Data With a Correlation and Jet Spreading Contours for a Large Variety of Nozzles. NASA TN D-8423, 1977.

25. Laurence, James C.: Intensity, Scale, and Spectra of Turbulence in Mixing Region of Free Subsonic Jet. NACA TR-1292, 1956.

26. Bradshaw, P.; Ferriss, D. H.; and Johnson, R. F.: Turbulence in the Noise-Producing Region of a Circular Jet. J. Fluid Mech., vol. 19, pt. 4, Aug. 1964, pp. 591-624.

27. von Glahn, U. H.; Groesbeck, D. E.; and Huff, R. G.: Peak Axial-Velocity Decay With Single- and Multi-Element Nozzles. NASA TM X-67979, 1972.

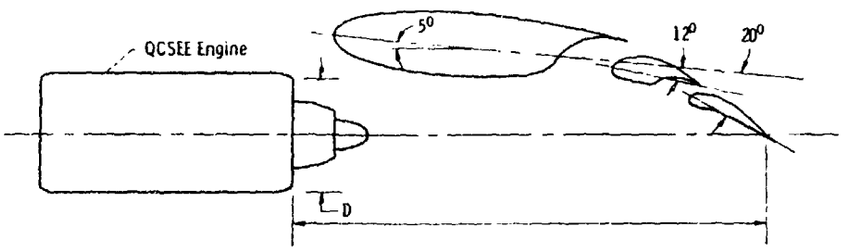

Figure 1. - QCSEE Configuration in the takeoff attitude x/D ~ 5.

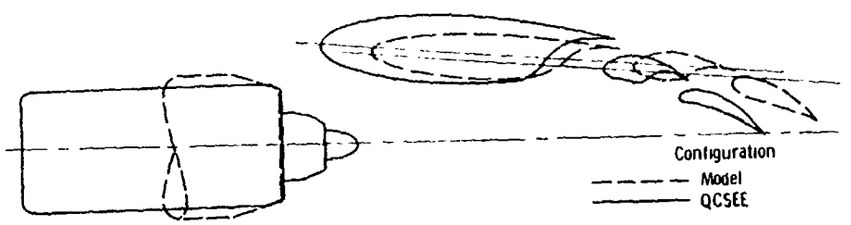

Figure 2. - Comparison between model and QCSEE EBF configurations in takeoff attitude.

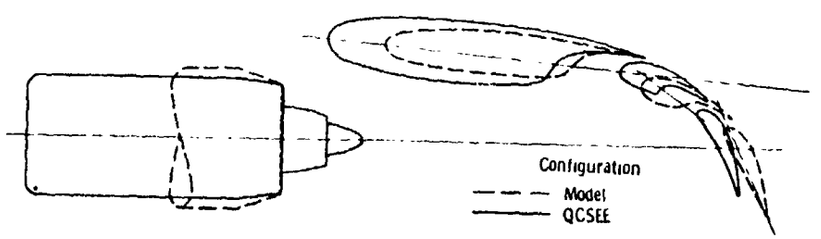

Figure 3. - Comparison between model and QCSEE EBF configurations in approach attitude.

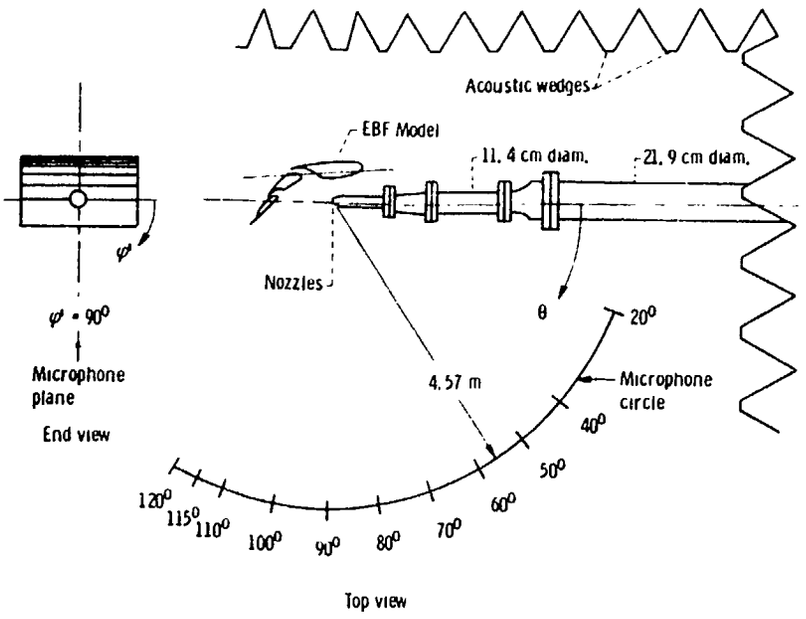

Figure 4. - Test rig in Engine Fan and Jet Noise Facility showing test model in flyover attitude, $\varphi = 90^{\circ}$.

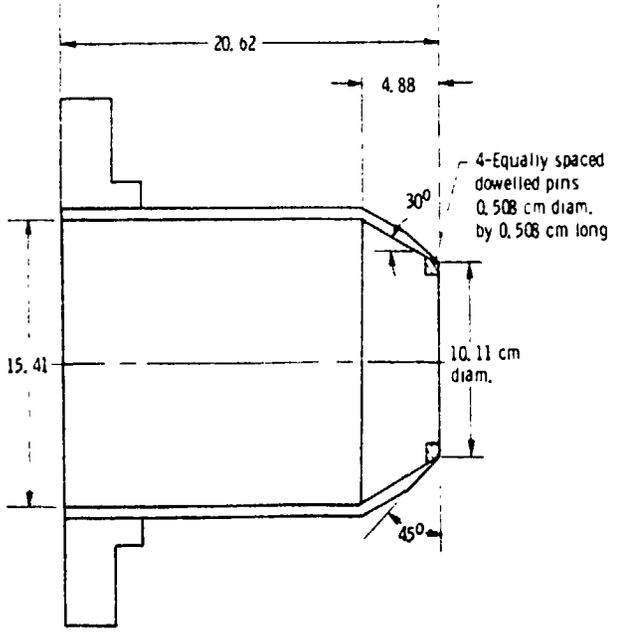

Figure 5. - Convergent nozzle with four pins in throat. All dimensions in centimeters.

TABLE I. - AERODYNAMIC PERFORMANCE CHARACTERISTICS OF UNSUPPRESSED AND SUPPRESSED CONFIGURATIONS

(a) Takeoff attitude; X/D = 4.9

Configuration	Mach number	Thrust coefficient, F_a/T	Lift coefficient, F_N/T	Turning efficiency, η	Turning angle, deg
Unsuppressed	0.5	0.74	0.22	0.77	16.6
	0.6	0.73	0.22	0.76	16.5
	0.7	0.75	0.21	0.78	15.9
Suppressed	0.5	0.74	0.20	0.76	14.8
	0.6	0.73	0.19	0.76	14.7
	0.7	0.74	0.20	0.76	14.8

(b) Approach attitudes; X/D = 4.0

Unsuppressed	0.5	0.32	0.45	0.56	54.6
	0.6	0.33	0.46	0.57	54.1
	0.7	0.34	0.46	0.57	53
Suppressed	0.5	0.32	0.43	0.53	53.3
	0.6	0.33	0.42	0.53	52.3
	0.7	0.34	0.41	0.53	50.3

TABLE II. - IMPACT NOISE IN FLYOVER PLANE FOR TAKEOFF INCIDENCE ANGLE ($\Psi_N = 20^\circ$). FLAT BOARD AT SEVEN-NOZZLE DIAMETERS SEPARATION; NOZZLE DIAMETER, D = 5.24 CM; MICROPHONE RADIUS, 3.05 M.

Jet impingement velocity, m/sec	Free field OASPL in dB at θ, deg								
	60	80	100	110	120	130	140	150	160
121.9	74	73.1	72.9	76.1	77.1	78.8	81.3	80.2	77.5
152.4	80.3	80.6	81.2	83.4	85	87.0	89.7	88.1	84.2
182.9	86.5	87.4	88.5	90.4	92.5	94.75	97.1	95.2	90.6
213.4	91.9	93	94.6	97.0	98.6	101	103.2	101	96.2
243.8	96.5	98.2	100.2	102.7	104	105.4	108.6	106.1	100.7
274.3	101.9	103.1	105.5	106.9	109.2	111.5	113.8	111	104

TABLE III. - IMPACT NOISE IN FLYOVER PLANE FOR APPROACH INCIDENCE ANGLE ($\Psi_N = 60^\circ$). FLAT BOARD AT FOUR-NOZZLE DIAMETERS SEPARATION; NOZZLE DIAMETER, D = 5.24 CM; MICROPHONE RADIUS, 3.05 M.

Jet impingement velocity, m/sec	Free field OASPL in dB at θ, deg								
	20	40	60	70	80	90	100	110	120
121.9	81.1	82.4	82.2	81.4	81.4	82.7	84.7	84.8	81.6
152.4	86.6	86.9	88	87.8	87.6	89.8	91.3	91	86.1
182.9	92	93.3	93.8	93.9	93.9	96.6	97.6	96.9	90.5
213.4	97.1	98.6	99.5	100	100.2	103	103.6	102.4	94.8
243.8	102	103.9	105.2	106.1	106.2	108.5	108.7	107.1	98.7
274.3	106.3	108.4	110	111.3	111.1	113	113.2	111.1	101.6

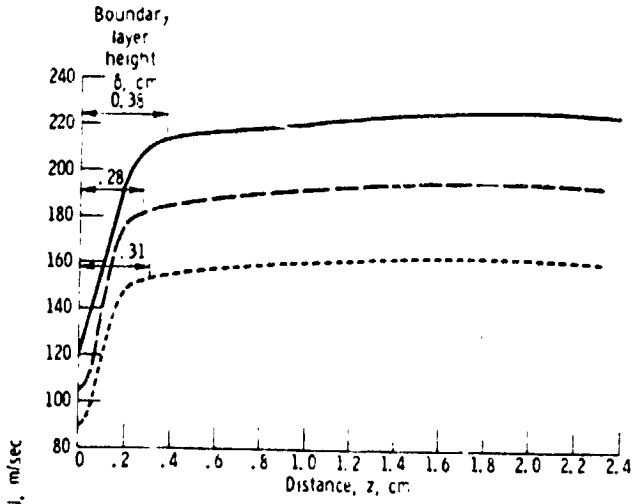

(a) Details of boundary layer region in plane of jet axis.

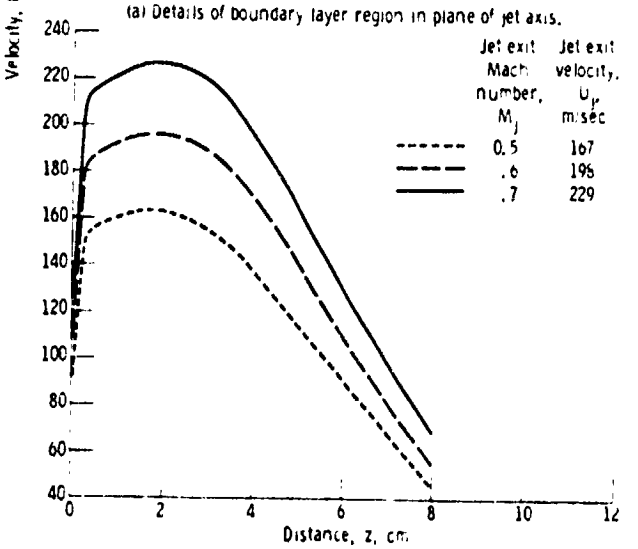

(b) Total shear layer in plane of jet axis.

Figure 10. - Measured velocity profiles at trailing edge of second flap of unsuppressed configuration in the takeoff attitude (x/D ~ 5).

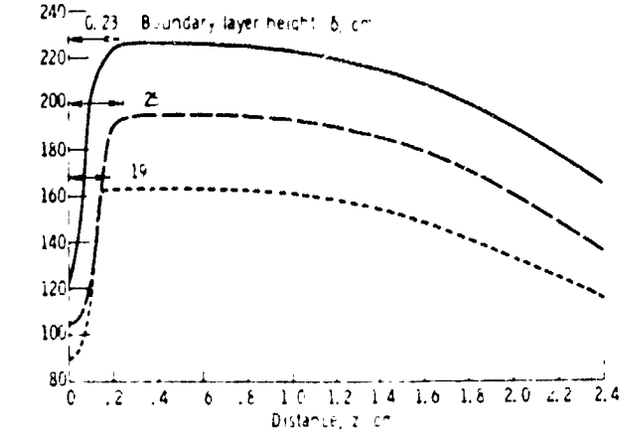

(a) Details of boundary layer region in plane of jet axis.

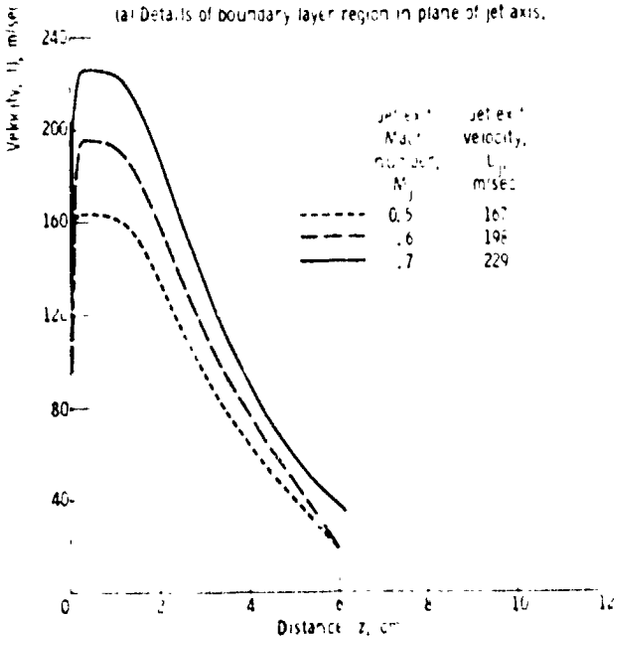

(b) Total shear layer in plane of jet axis

Figure 11 - Measured velocity profiles at trailing edge of second flap of unsuppressed configuration in approach attitude (x/D = 4).

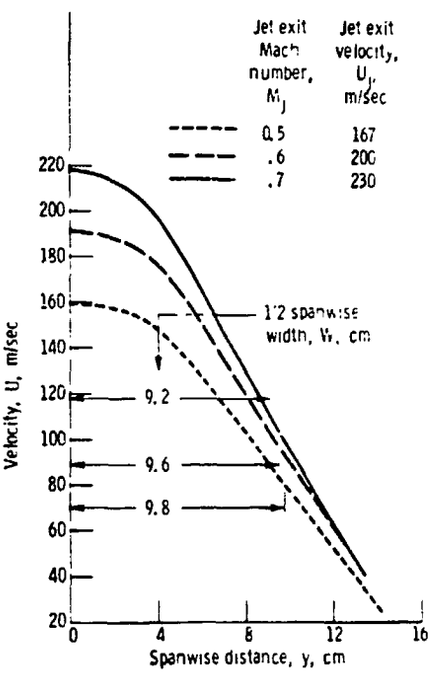

(c) Spanwise velocity profiles at z of 1.0 centimeters.

Figure 11. - Concluded.

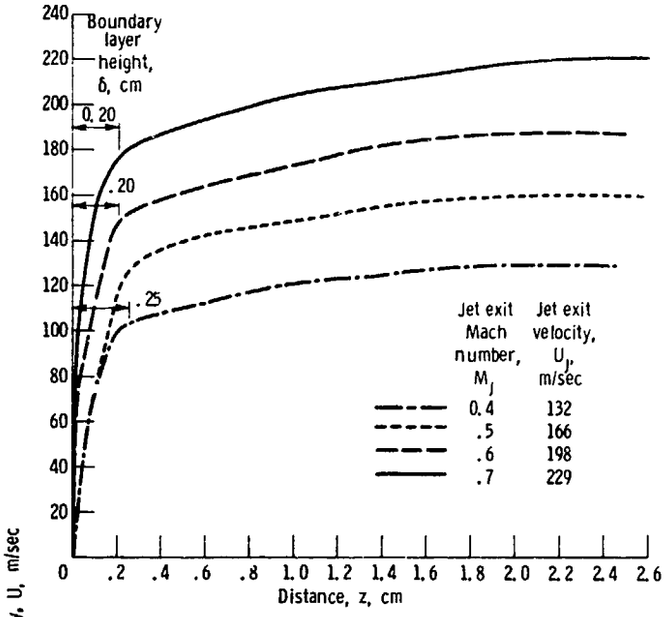

(a) Detail of boundary layer region in plane of jet axis.

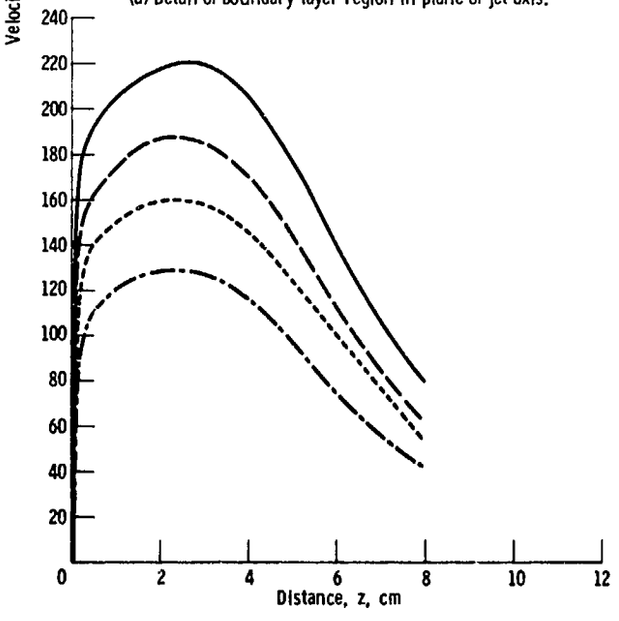

(b) Total shear layer in plane of jet axis.

Figure 12. - Measured velocity profiles at trailing edge of second flap of the suppressed configuration in the takeoff attitude (x/D = 4).

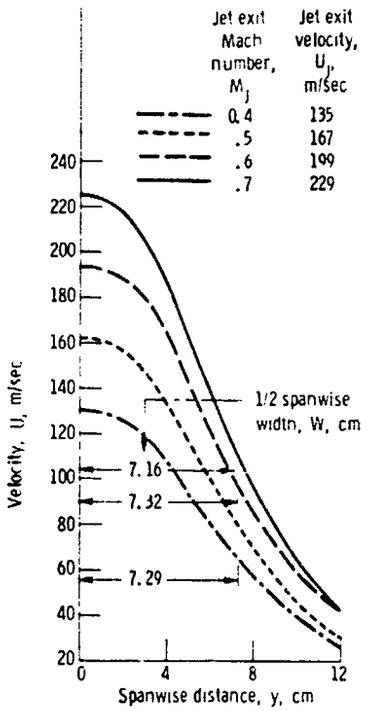

(c) Spanwise velocity profile at z of 2.67 centimeters.

Figure 12. - Concluded.

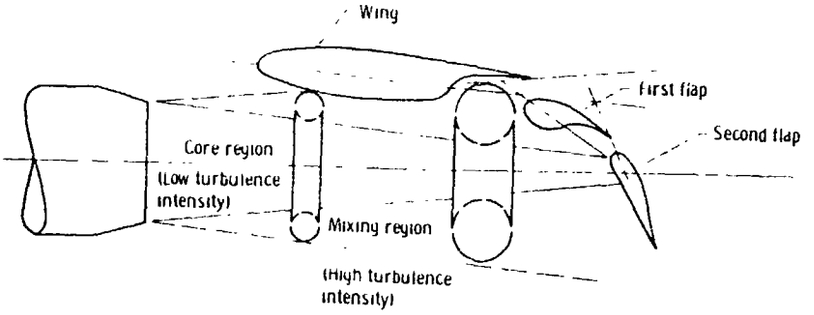

Figure 13. - Schematic diagram of interaction of large-scale turbulence structure with EBF unsuppressed configuration in approach attitude.

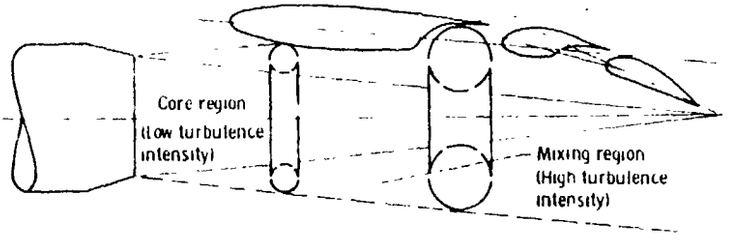

Figure 14. - Schematic diagram of interaction of large-scale turbulence structure with EBF unsuppressed configuration in takeoff attitude.

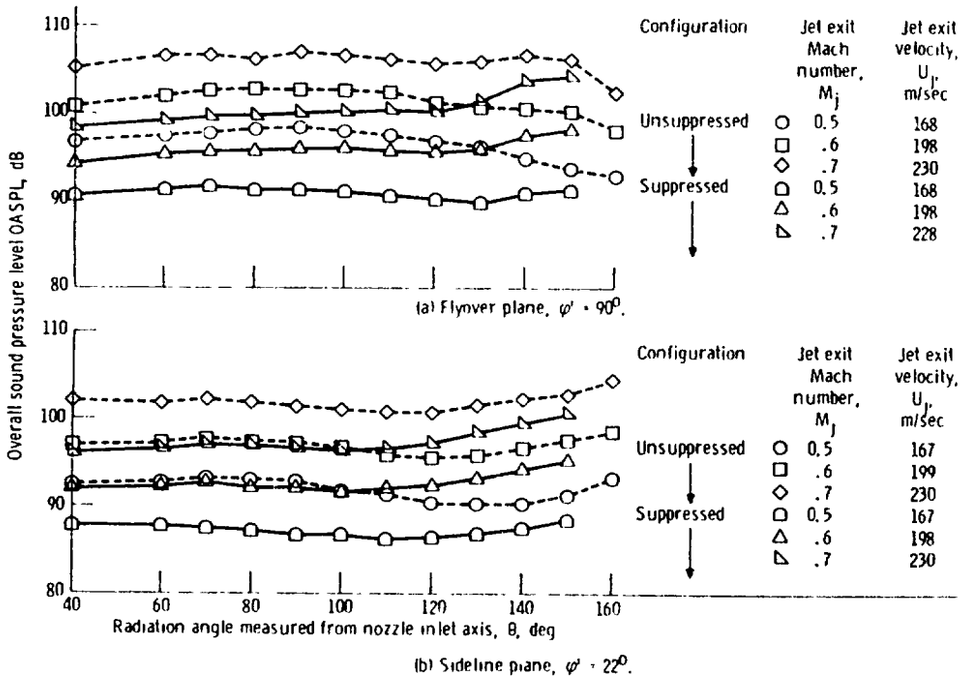

Figure 15. - Comparison of overall sound pressure level for unsuppressed and suppressed configurations in takeoff attitude

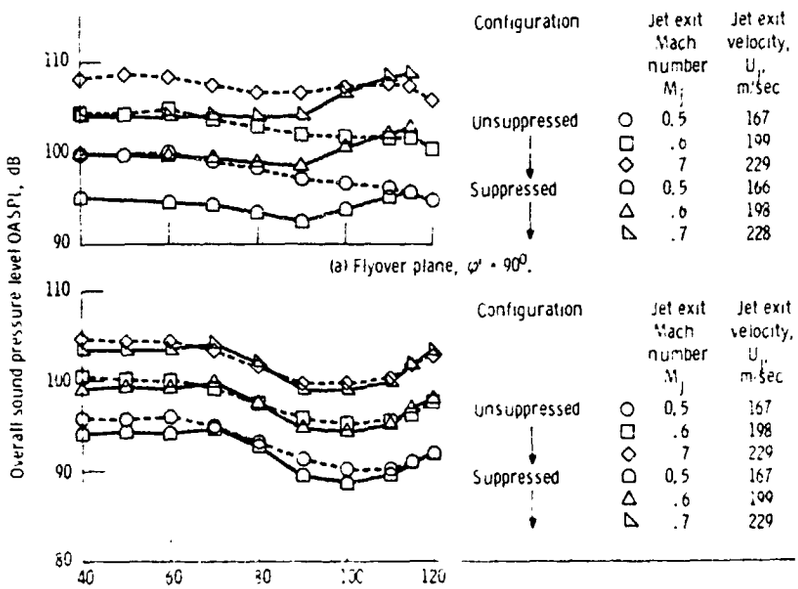

Figure 16. - Comparison of overall sound pressure level for unsuppressed and suppressed configurations in approach attitude.

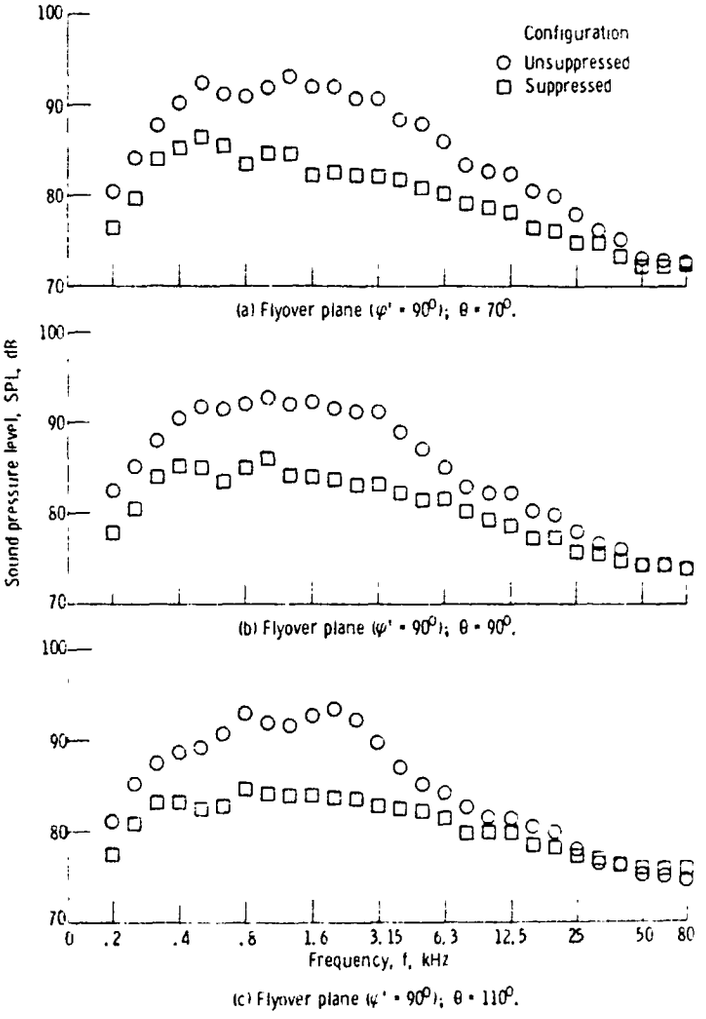

Figure 17. - Comparison of sound pressure level for unsuppressed and suppressed configurations in takeoff attitude at a jet Mach number, M_j, of 0.6.

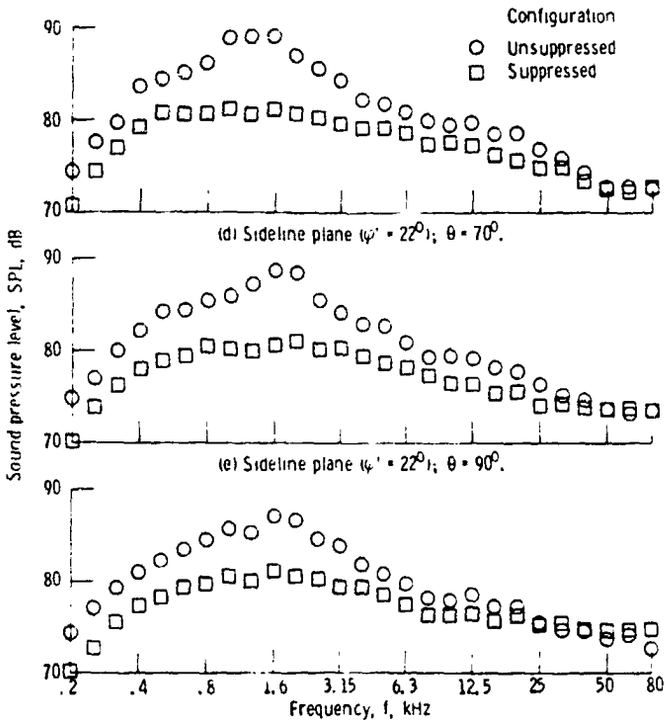

(d) Sideline plane ($\varphi' = 22^0$); $\theta = 70^0$.

(e) Sideline plane ($\varphi' = 22^0$); $\theta = 90^0$.

(f) Sideline plane ($\varphi' = 22^0$); $\theta = 110^0$.

Figure 17. - Concluded.

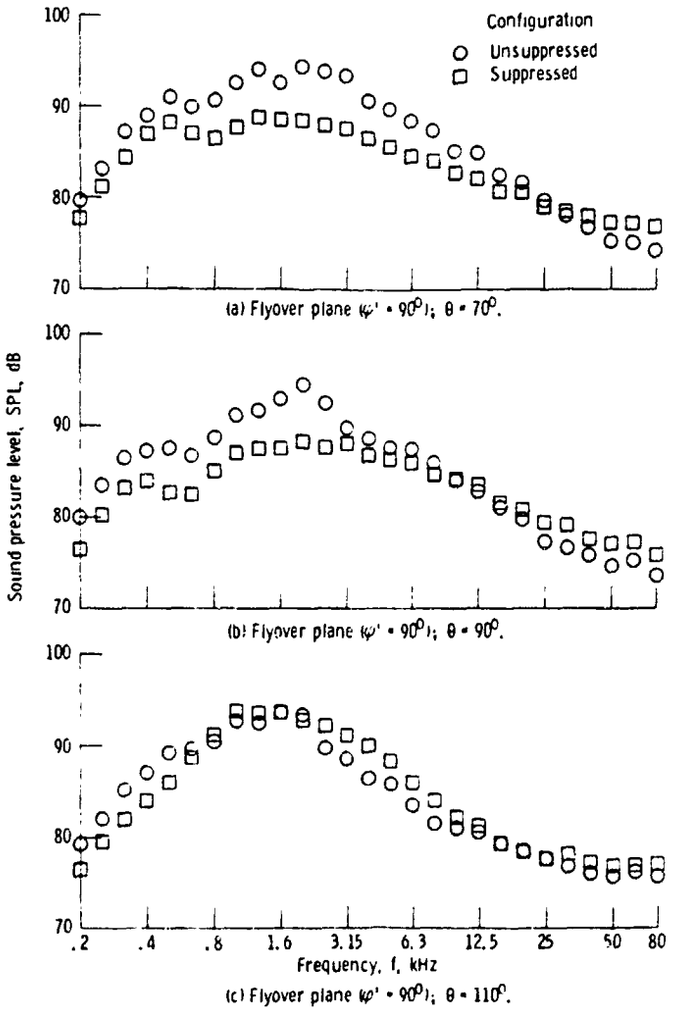

Figure 18. - Comparison of sound pressure level for unsuppressed and suppressed configurations in approach attitude at a jet Mach number, M_j, of 0.6.

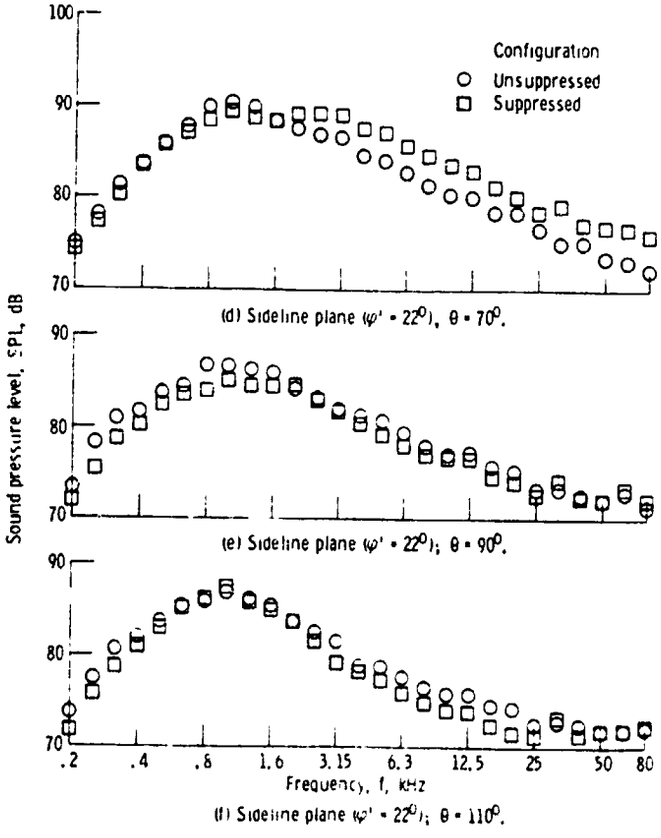

(d) Sideline plane $(\varphi' = 22^0)$, $\theta = 70^0$.

(e) Sideline plane $(\varphi' = 22^0)$; $\theta = 90^0$.

(f) Sideline plane $(\varphi' = 22^0)$; $\theta = 110^0$.

Figure 18. - Concluded.

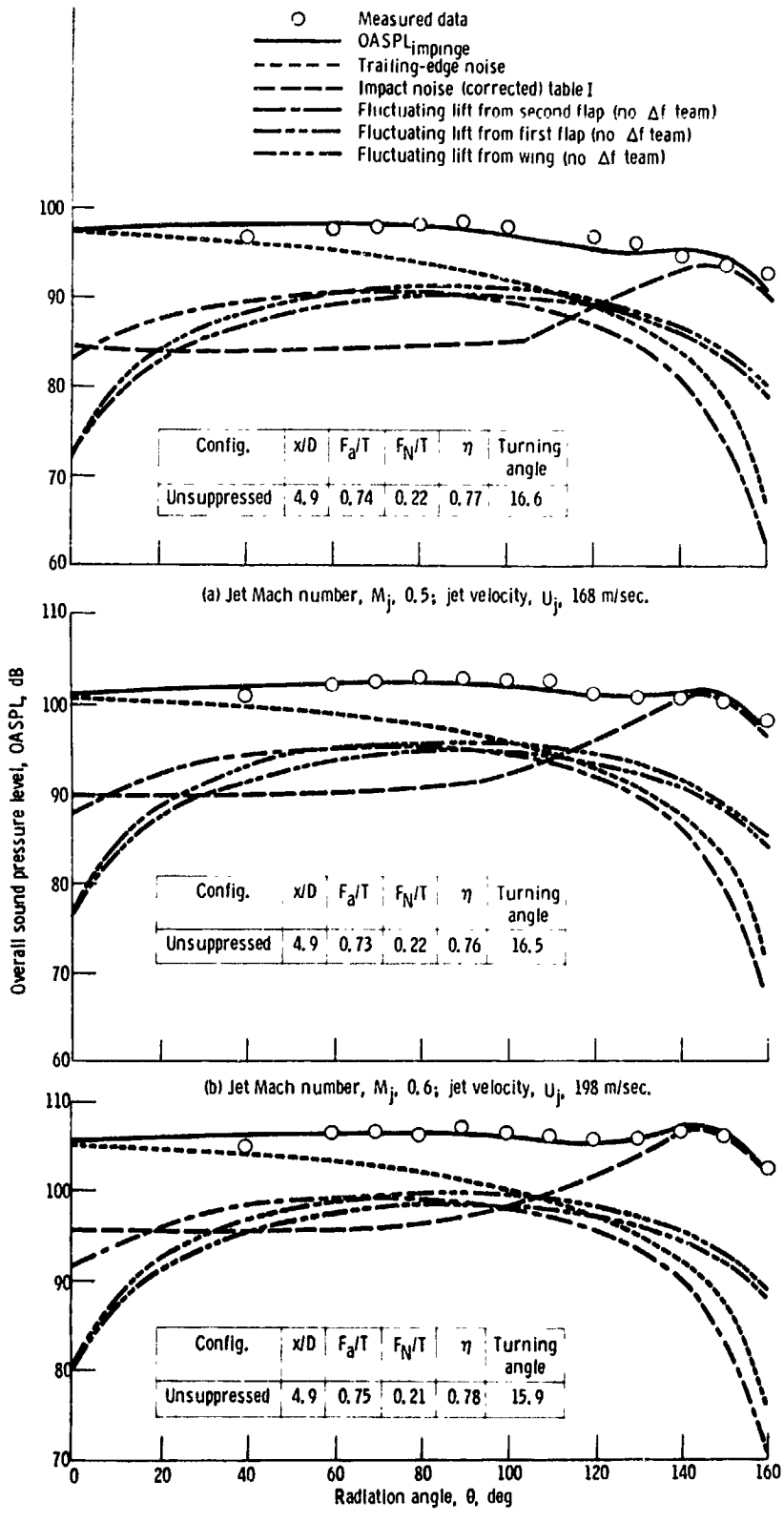

(a) Jet Mach number, M_j, 0.5; jet velocity, U_j, 168 m/sec.

(b) Jet Mach number, M_j, 0.6; jet velocity, U_j, 198 m/sec.

(c) Jet Mach number, M_j, 0.7; jet velocity, U_j, 230 m/sec.

Figure 19. - Comparison of measured and calculated overall sound pressure level for unsuppressed configuration in takeoff attitude. Flyover plane, $\varphi' = 90^0$.

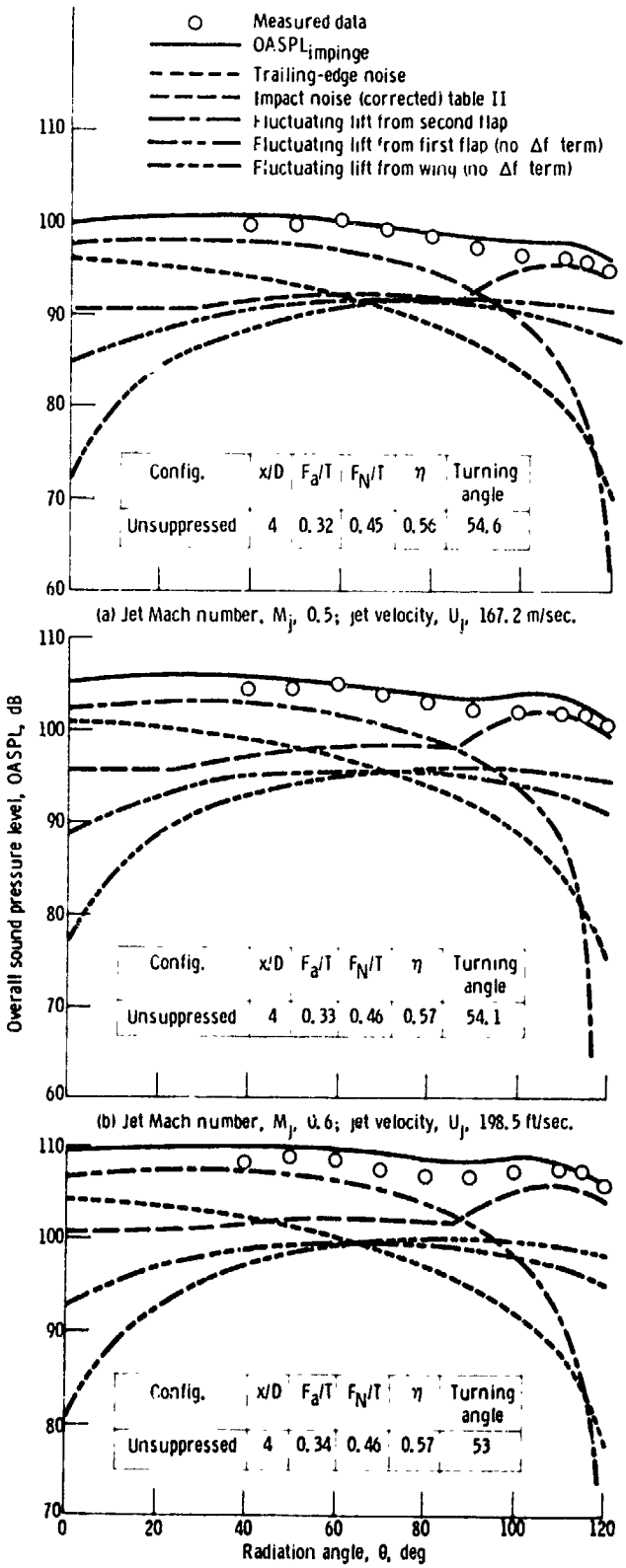

(a) Jet Mach number, M_j, 0.5; jet velocity, U_j, 167.2 m/sec.

(b) Jet Mach number, M_j, 0.6; jet velocity, U_j, 198.5 ft/sec.

(c) Jet Mach number, M_j, 0.7; jet velocity, U_j, 228.5 ft/sec.

Figure 20. - Comparison of measured and calculated overall sound pressure level for unsuppressed configuration in approach attitude. Flyover plane, $\varphi' = 90^0$.

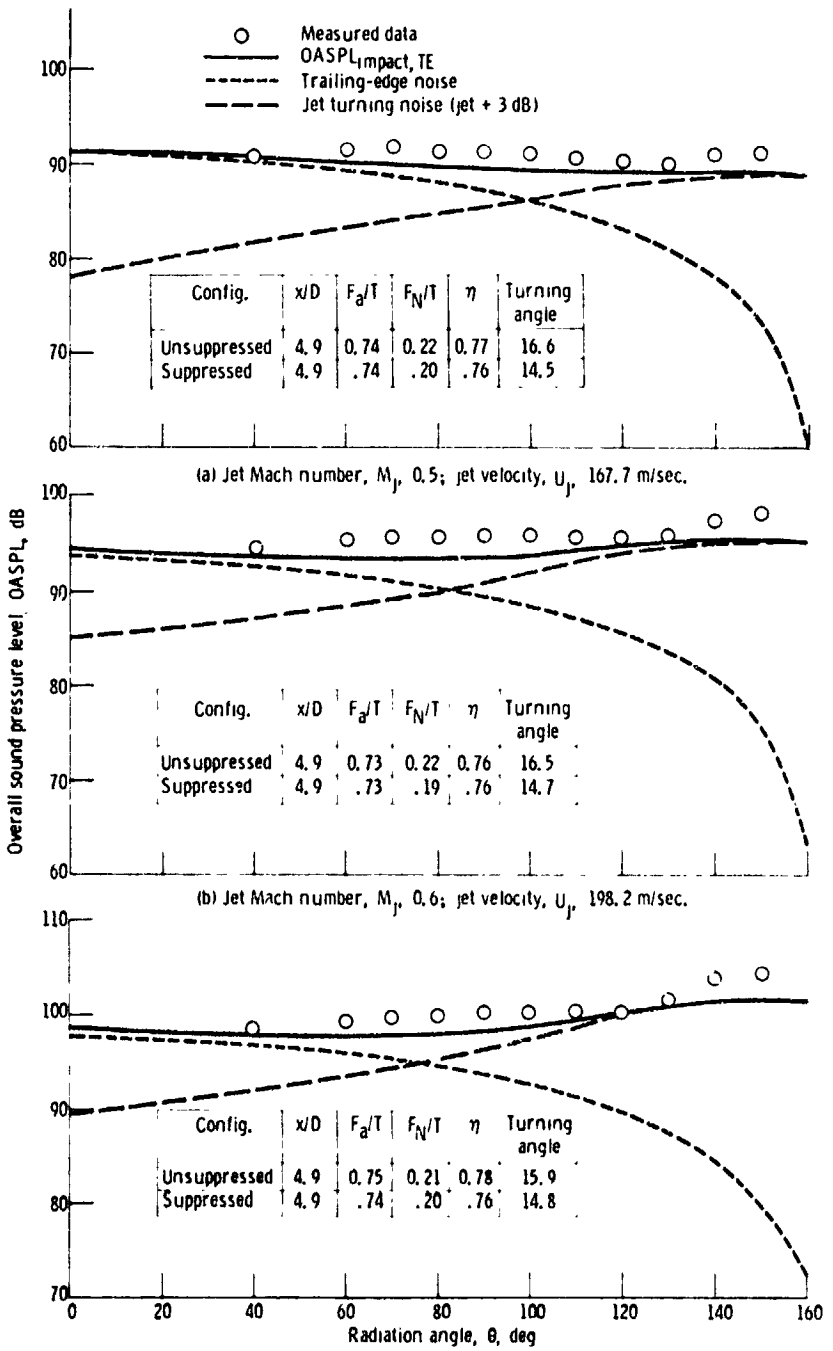

(a) Jet Mach number, M_j, 0.5; jet velocity, U_j, 167.7 m/sec.

(b) Jet Mach number, M_j, 0.6; jet velocity, U_j, 198.2 m/sec.

(c) Jet Mach number, M_j, 0.7; jet velocity, U_j, 228.1 m/sec.

Figure 21. - Comparison of measured and calculated overall sound pressure level for suppressed configuration in takeoff attitude. Flyover plane, $\psi' = 90^0$.

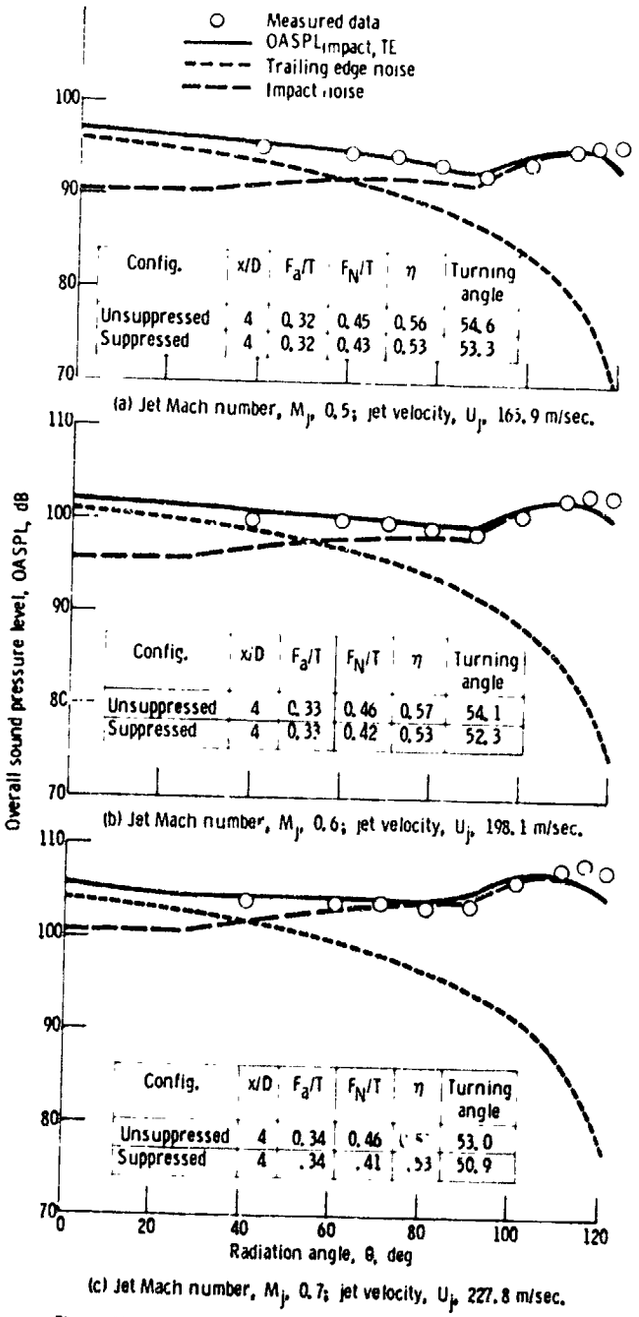

(a) Jet Mach number, M_j, 0.5; jet velocity, U_j, 163.9 m/sec.

(b) Jet Mach number, M_j, 0.6; jet velocity, U_j, 198.1 m/sec.

(c) Jet Mach number, M_j, 0.7; jet velocity, U_j, 227.8 m/sec.

Figure 22. - Comparison of measured and calculated overall sound pressure level for suppressed configuration in approach attitude. Flyover plane, $\varphi' = 90^0$.

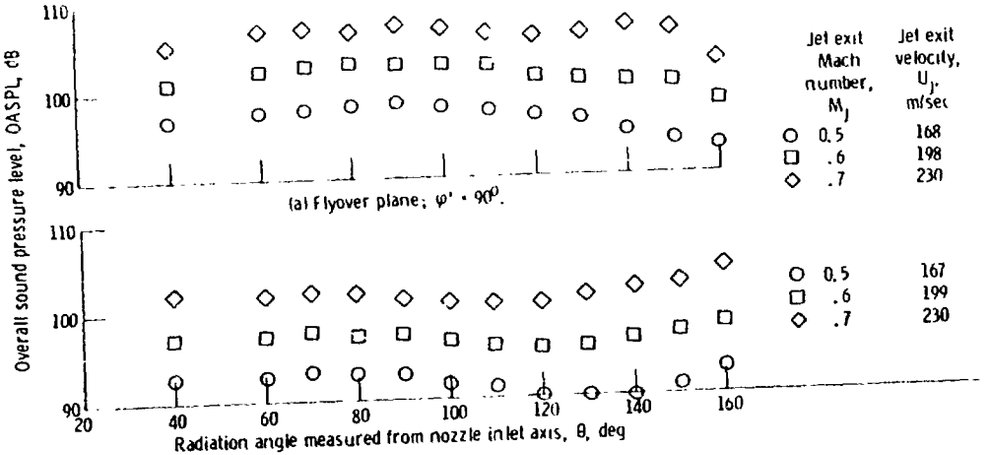

Figure 23. - Overall sound-pressure level distribution for unsuppressed configuration in takeoff attitude.

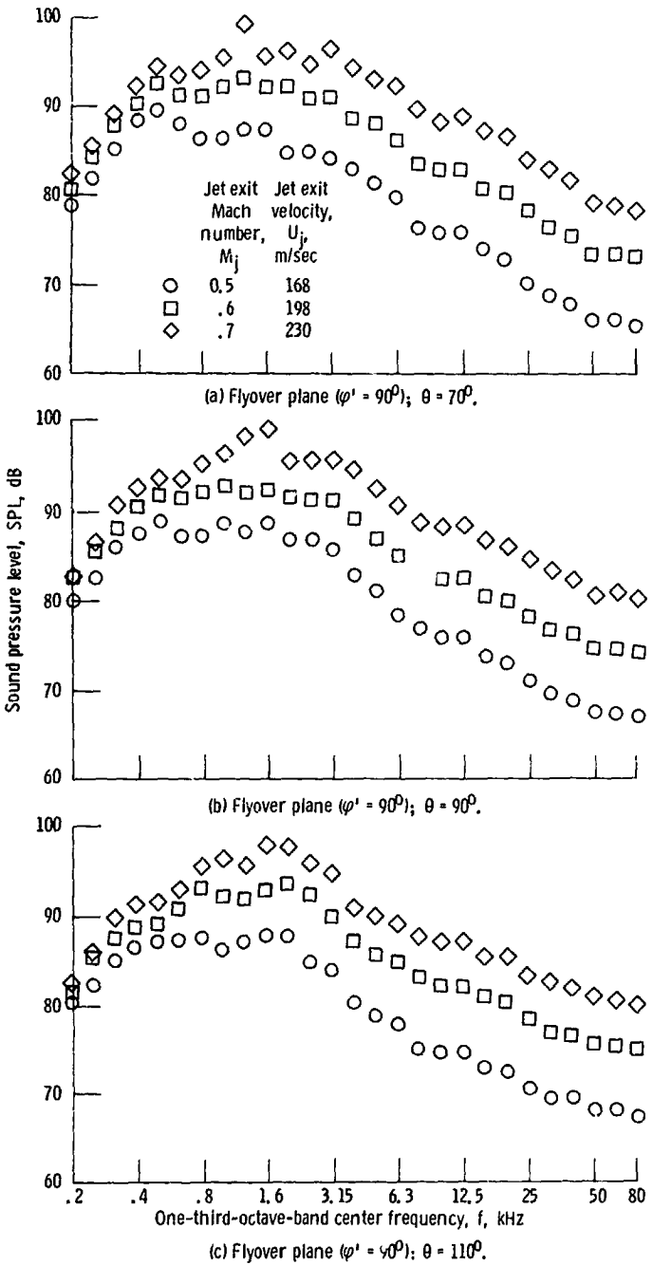

(a) Flyover plane ($\varphi' = 90^0$); $\theta = 70^0$.

(b) Flyover plane ($\varphi' = 90^0$); $\theta = 90^0$.

(c) Flyover plane ($\varphi' = 90^0$); $\theta = 110^0$.

Figure 24. - Sound-pressure-level distribution for unsuppressed configuration in takeoff attitude.

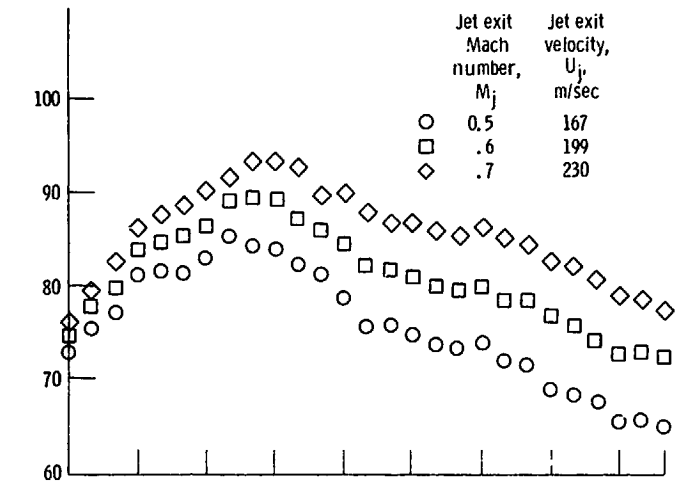

(d) Sideline plane ($\varphi' = 22^0$); $\theta = 70^0$.

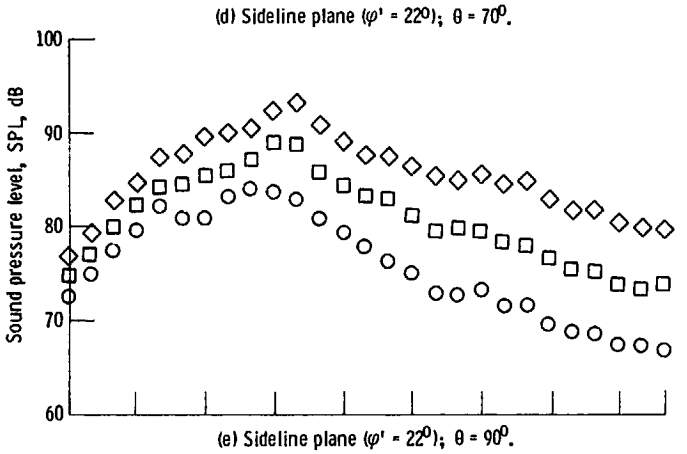

(e) Sideline plane ($\varphi' = 22^0$); $\theta = 90^0$.

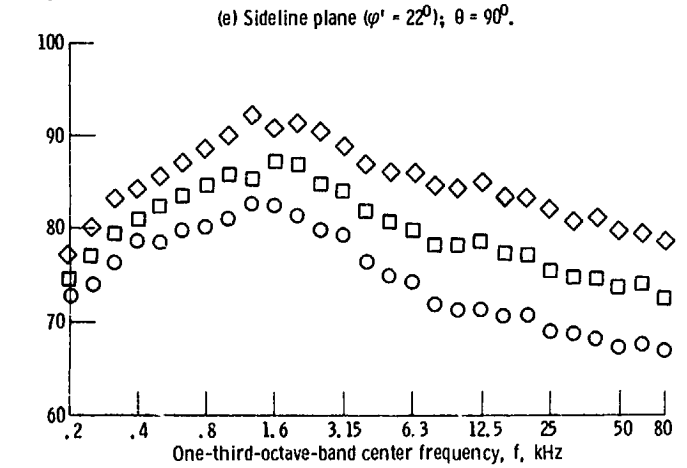

(f) Sideline plane ($\varphi' = 22^0$); $\theta = 110^0$.

Figure 24. - Concluded.

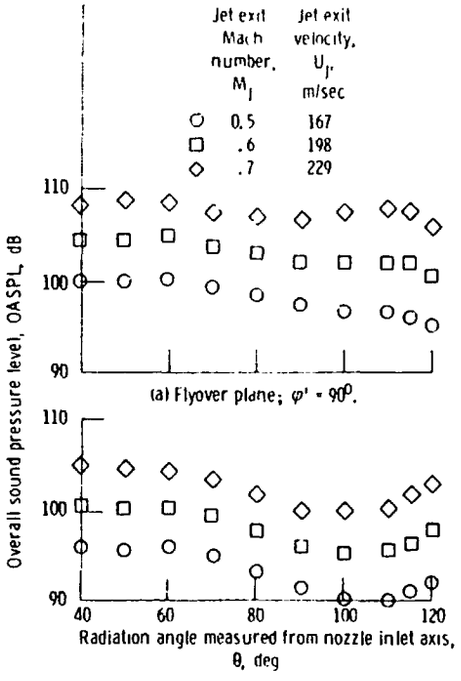

(a) Flyover plane; $\varphi' = 90^0$.

(b) Sideline plane; $\varphi' = 22^0$.

Figure 25. - Overall-sound-pressure-level distribution for unsuppressed configuration in approach attitude.

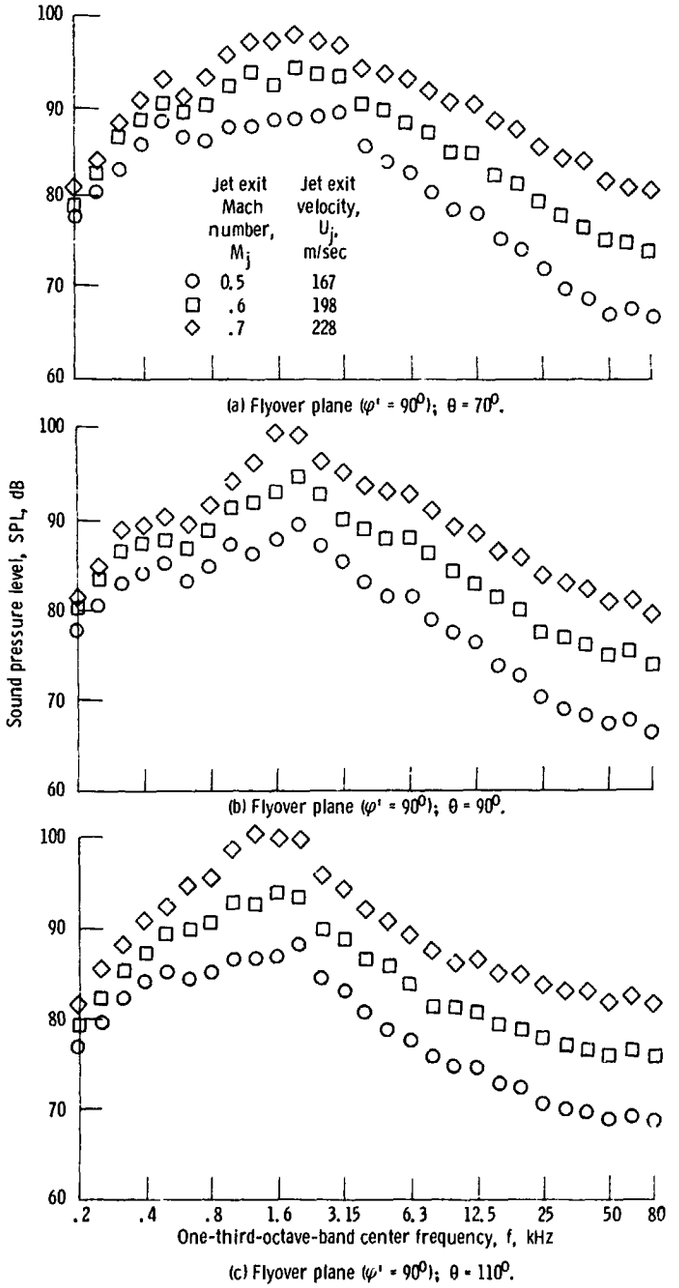

(a) Flyover plane ($\varphi' = 90^0$); $\theta = 70^0$.

(b) Flyover plane ($\varphi' = 90^0$); $\theta = 90^0$.

(c) Flyover plane ($\varphi' = 90^0$); $\theta = 110^0$.

Figure 26. - Sound-pressure-level distribution for unsuppressed configuration in approach attitude.

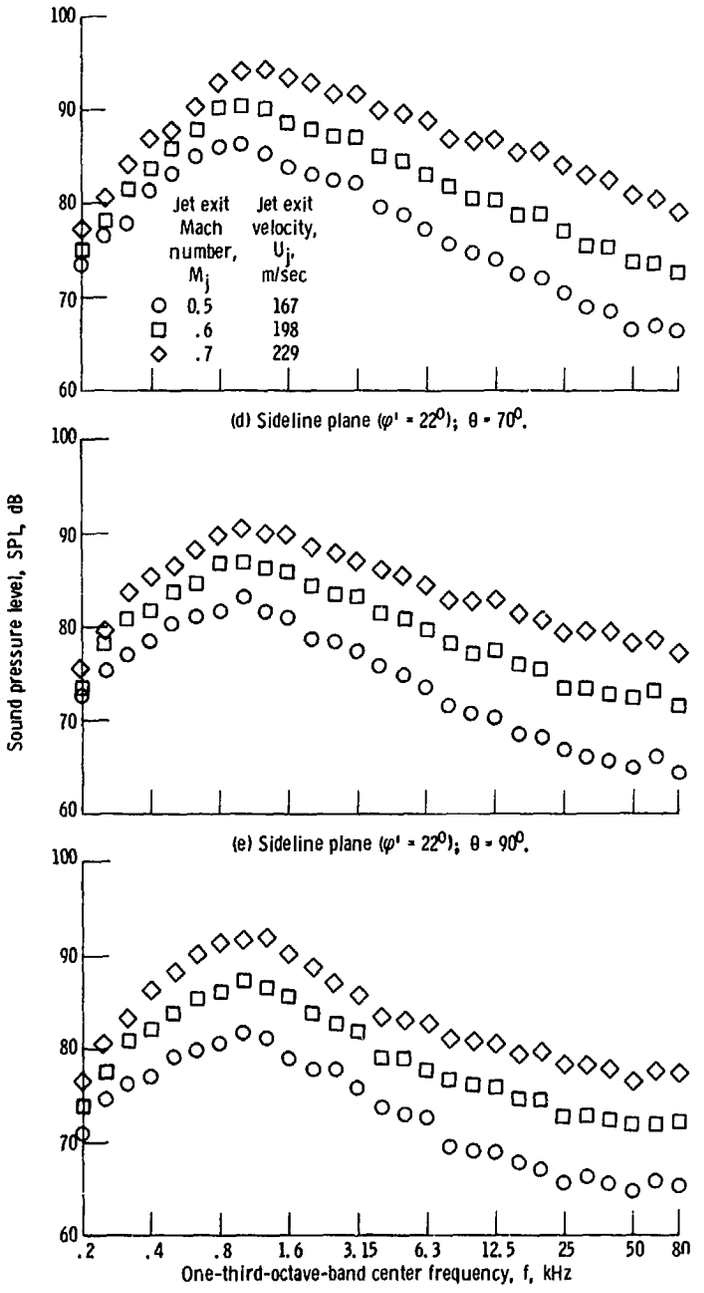

(d) Sideline plane ($\varphi' = 22^0$); $\theta = 70^0$.

(e) Sideline plane ($\varphi' = 22^0$); $\theta = 90^0$.

(f) Sideline plane ($\varphi' = 22^0$); $\theta = 110^0$.

Figure 26. - Concluded.

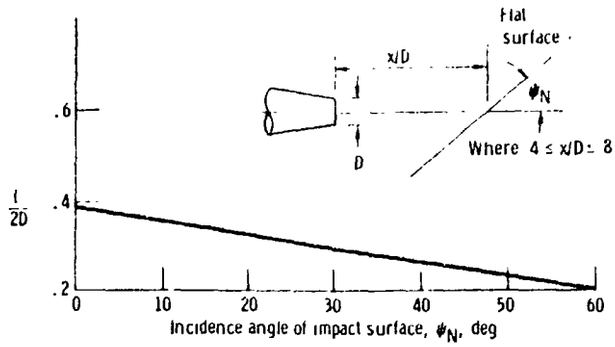

Figure 27. - Lateral correlation length L for oblique impingement of a large-scale jet turbulence structure against a flat surface. Based on measured data from refs. 1, 23, and 24.

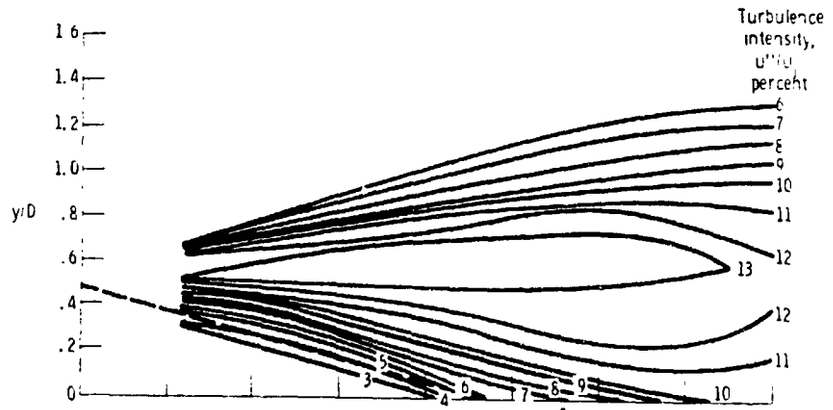

(a) Axial component u''/U_j in percent at $Re = 3 \times 10^5$; $M_j = 0.3$; ref. 28.

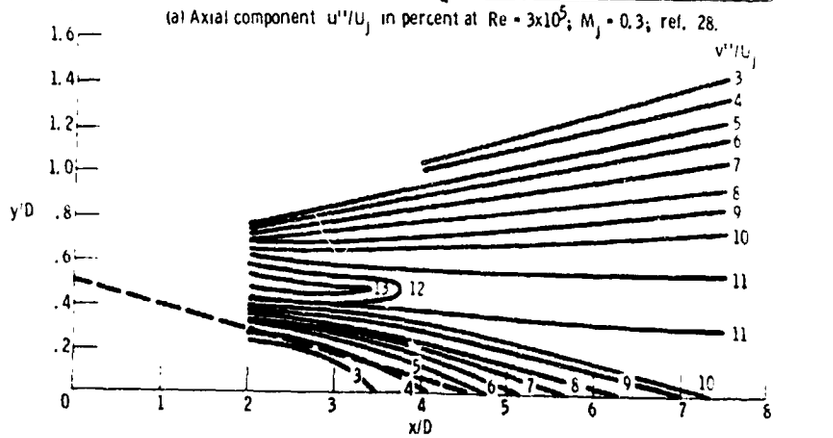

(b) Radial component v''/U_j in percent at M_j of 0.3; ref. 26.

Figure 28. - Axial and radial components of circular jet turbulence intensities.

1 Report No NASA TM-81494	2 Government Accession No	3 Recipient's Catalog No
4 Title and Subtitle MEASURED AND PREDICTED IMPINGEMENT NOISE FOR A MODEL-SCALE UNDER-THE-WING EXTERNALLY BLOWN FLAP CONFIGURATION WITH A QCSEE-TYPE NOZZLE		5 Report Date June 1980 6 Performing Organization Code
7 Author(s) D. J. McKinzie, Jr.		8 Performing Organization Report No E-432 10. Work Unit No
9 Performing Organization Name and Address National Aeronautics and Space Administration Lewis Research Center Cleveland, Ohio 44135		11 Contract or Grant No 13 Type of Report and Period Covered Technical Memorandum
12 Sponsoring Agency Name and Address National Aeronautics and Space Administration Washington, D.C. 20546		14 Sponsoring Agency Code
15 Supplementary Notes		

16 Abstract

Jet flap interaction noise was measured and predicted for a small-scale model two-flap, under-the-wing (UTW), externally blown flap (EBF) configuration equipped with and without noise suppression devices. The devices consisted of short spanwise fairings centered in relationship to the jet axis and positioned in the slots between the wing and flaps. The nozzle approximated that of the Quiet Clean Short-haul Experimental Engine (QCSEE). Takeoff noise reductions of 6 dB in the flyover and 5 dB in the sideline plane were obtained over a wide range of radiation angles. Approach noise reductions of about 5 dB were obtained only in the forward quadrant of the flyover plane; no reductions were obtained in the sideline plane. Models of several noise sources were combined analytically to form an overall noise prediction, the results from which compared favorably with the measured data. The aerodynamic performance characteristics for these configurations were substantially the same in the takeoff attitude. However, in the approach attitude, the suppressed configuration produced a 6-percent reduction in the flow turning efficiency.

17 Key Words (Suggested by Author(s)) Acoustics V/STOL Propulsion Noise	18 Distribution Statement Unclassified - unlimited STAR Category 71		
19 Security Classif (of this report) Unclassified	20 Security Classif (of this page) Unclassified	21. No of Pages	22 Price*

* For sale by the National Technical Information Service Springfield Virginia 22161